Structural analysis of non-prismatic beams: critical issues, accurate stress recovery, and analytical definition of the Finite Element (FE) stiffness matrix

Valentina Mercuri[a], Giuseppe Balduzzi[b,*], Domenico Asprone[c], Ferdinando Auricchio[d]

[a] *Freelance Enigneer, Montefalcone Appennino, Italy*
[b] *Institute for Mechanics of Materials and Structures (IMWS), Vienna University of Technology, Vienna, Austria*
[c] *Department of Structures for Engineering and Architecture, University of Naples Federico II, Naples, Italy*
[d] *Department of Civil Engineering and Architecture (DICAr), University of Pavia, Pavia, Italy*

Abstract

Non-prismatic beams are widely employed in strategic structures like bridges and sport arenas, requiring accurate analyses for a reliable and effective design. Unfortunately, features of non-prismatic beams lead their modeling to be a non-trivial task: (i) variations of both cross-section area and second moment of area impede an easy computation of analytical solutions compelling to use approximated methods; (ii) stress distributions in prismatic and non-prismatic beams are substantially different, as proved by analytical results available since the beginning of the past century; and (iii) the peculiar stress distribution in non-prismatic beams entails complicated constitutive relations, as highlighted in recent publications. Usually, commercial software does not properly account for all the features of non-prismatic beams, leading to inconsistent structural analyses, erroneous estimations of the stress distribution, and -consequently- coarse predictions of the structural element strength. The present paper proposes a strategy to effectively overcome the above-mentioned problems. We derive an accurate analytical model for 2D non-prismatic beams, able to handle the non-trivial stress distribution and the complicated constitutive relations. Thereafter, we compute both homogeneous and particular solutions using the symbolic calculus software MAPLE and we analytically define the Finite Element (FE) stiffness matrix for a planar, symmetric, linearly-tapered beam. Finally, we compare the proposed FE and SAP2000 solutions, considering several beams with different geometries, loads, and constraints. Numerical results highlight the reliability of the proposed modeling strategy, since the resulting FE consistently handles all the critical issues of non-prismatic beams with an extremely low computational cost. Conversely, SAP2000 solution remarks the need of ad hoc analysis tools and modeling strategies to be used for the design of non-prismatic structural elements.

Keywords: Non-prismatic Beam FE, Haunch Beams, Tapered Beam Model, Stiffness Matrix Analytical Definition, Reinforced Concrete Frames

*Corresponding author. *Address*: Institute for Mechanics of Materials and Structures (IMWS), Vienna University of Technology, Karlsplatz 13/202 A-1040 Vienna, Austria *Email address*: Giuseppe.Balduzzi@tuwien.ac.at *Phone*: 0043 (1) 58 80 12 02 28

Email addresses: ing.valentinamercuri@gmail.com (Valentina Mercuri), Giuseppe.Balduzzi@tuwien.ac.at (Giuseppe Balduzzi), domenico.asprone@unina.it (Domenico Asprone), auricchio@unipv.it (Ferdinando Auricchio)

1. Introduction

Non-prismatic structural elements are widely used in civil engineering since they allow to optimize the structural behavior with respect to architectural and functional requirements, reducing structure weight, material consumption, environmental impact, and costs. Limiting the attention to Reinforced Concrete (RC) structures, non-prismatic beams are successfully employed in viaducts and bridges [16], industry roofing [22], and multi-stories buildings [63]. Structural elements with variable cross-section are also experiencing a renewed interest in the framework of geometrically optimized RC structures [3, 74]. Furthermore, additive-manufacturing, a fast-developing technology, allows to bypass standard manufacturing constraints, opening the path to a new generation of structures [71] and compelling for enhanced modeling.

Oddly, Paglietti and Carta [47] and Beltempo et al. [16] reported non-predicted and undesired phenomena in non-prismatic RC structural elements, suggesting that their mechanical behavior is not as trivial as expected. Furthermore, Paglietti and Carta [48], Yang et al. [73], and Orr et al. [46] noticed critical issues in the procedures usually employed for the design of RC non-prismatic beams, indicating that analysis tools for non-prismatic beams still need substantial improvements.

The present paper aims at (i) overcoming the critical issues discussed above, and (ii) improving the design of non-prismatic structural elements by means of simple, consistent, and reliable models.

The remaining part of this section presents a detailed discussion of the problems occurring in the structural analysis of non-prismatic beams, for both continuous 1D models (Subsection 1.1) and numerical discretization (Subsection 1.2). Section 2 derives (i) an effective procedure for the recovery of stress distribution, (ii) a former non-prismatic planar beam model (denoted in the following as full Non-Prismatic Beam Model (NPBM)) according to the derivation path proposed by Beltempo et al. [15] and accounting for the novel stress recovery, and (iii) a latter beam model (denoted in the following as simplified NPBM), obtained linearizing the full NPBM with respect to several parameters and allowing for the handling of both homogeneous and particular analytical solutions. Section 3 discusses few numerical examples taken from the literature for the validation of the proposed models. Section 4 derives analytical expressions for the Finite Element (FE) stiffness matrix coefficients on the basis of the simplified NPBM analytical solution and exploiting the analogy between direct stiffness and FE methods. Section 5 compares the obtained stiffness matrix with the well-known software SAP2000 [25] (taken as example in the wide range of commercial software for structural analysis) and highly-refined 2D FE analysis performed using Abaqus [61] (used as reference solution). Finally, Section 6 discusses conclusions and delineates future developments.

The rigorous derivation path of NPBM allows to develop accurate and consistent analysis tools. Furthermore, NPBM based FE presents an extremely low computational cost since it discretizes one non-prismatic structural element with just one FE, without the need of any mesh refinements. Conversely, commercial software results highlight gaps in post-processing and design tools that are not able to describe the peculiar stress distribution of non-prismatic beams and a coarse estimation of structural element stiffness, in particular for high taper ratio and low slenderness.

1.1. Continuous 1D models

The simplest modeling approach for non-prismatic beams consists of modifying the Euler-Bernoulli or the Timoshenko beam Ordinary Differential Equations (ODEs). Both the above mentioned models are derived for prismatic bodies i.e., for beams with constant axial, shear, and bending stiffnesses (proportional to cross-section area and second moment of area) [24]. Non-prismatic beam model is obtained just substituting the constant stiffness coefficients of prismatic beam ODEs with functions accounting for the variations of cross-section area and second moment of area [65, 52, 78, 69, 72]. This apparently trivial modification of the beam model however leads to ODEs for which an explicit analytical solution is difficult to compute. Indeed, in standard beam models, constitutive relations define curvature, axial, and shear deformations as the quotients of bending moment, axial, and transversal internal forces divided by the corresponding stiffnesses. Therefore, if the stiffness varies, generalized deformations turn out being rational functions and their primitive integrals (necessary for the displacement evaluation) cannot be easily computed. In particular, (i) polynomial solutions exist and can be easily computed only if bending, axial, and shear stiffness are inversely proportional to the axial coordinate, [78, Example 10.11]; (ii) the analytical solution contains

rational polynomials and logarithmic functions even for a simple tapered beam with a linear variation of the cross-section thickness [57]; and (iii) the analytical solution cannot be computed for arbitrarily complicated geometries.

In the past, when computers were not available, such a situation forced practitioners to use approximated approaches e.g., tabular coefficients and charts for the estimation of non-prismatic beam stiffness [52] and beam maximal displacements [51, 59]. Despite still widely used in everyday practice, such simplified strategies are inadequate for nowadays engineering standard. Indeed, El-Mezaini et al. [28], Balkaya et al. [14], and Al-Ghatani and Khan [1] indicate that tabular coefficients reported in [52] lead to a rough estimation of the structural element stiffness, while Balduzzi et al. [11] demonstrate that estimations of beam maximal displacements provided by Schneider et al. [59] can be affected by non-negligible errors.

The motivations for such errors in the simplest modeling approach can be partially addressed considering the analytical solution of 2D equilibrium Partial Differential Equations (PDEs) for an infinite-long wedge [64, Article 35]. Trahair and Ansourian [66], Balduzzi et al. [10], and Bennati et al. [17] highlight that, according to the just mentioned analytical solution, a linear variation of the beam thickness drastically modifies the stress distribution within the cross-section. As an example, a pure bending load applied to a linearly-tapered beam leads to a non-vanishing (and non-negligible) distribution of shear stress [10, Section 1.1]. The non-trivial dependence of shear stress on bending moment (and axial internal force) can also be inferred from the equilibrium Boundary Condition (BC) on the beam lateral surface. Since the normal unit vector on the lateral surface is generally not perpendicular to the beam axis, equilibrium BC does not lead the shear stress to vanish at the cross-section lower and upper boundaries (as usual in prismatic beams), but to be proportional to the axial stress and the slope of the lateral surface [35, 9]. Similar considerations can be generalized to beams with different peculiarities. As an example, Balduzzi et al. [8] demonstrated that a non vanishing distribution of shear stress occurs also in a Functionally Graded Material (FGM) beam with non-linear variation of the mechanical properties subjected to pure bending. However, also in this research field, the dependence of shear stress on bending moment and horizontal internal force is not addressed in a proper way [39, 43].

Several methods aiming at overcoming the so-far introduced critical issue have been proposed since the beginning of the past century. As an example, the theory of shear strength proposed by Bleich [19], the formula derived by Vu-Quoc and Léger [70], and the approach proposed by Zhou et al. [77] discuss stress recovery procedures specific for non-prismatic beams. However, Paglietti and Carta [48] highlight that the theory of shear strength leads to contradictory results, while Balduzzi et al. [10] demonstrate that the recovery approach proposed in [70] may lead to rough estimations of the shear stress distribution. Such a fundamental problem has been properly addressed only in recent years: Balduzzi et al. [7] have proposed an effective recovery procedure based on Jourawski approach [36] and equilibrium BC for planar multi-layer non prismatic beams, while Bertolini et al. [18] used the 3D equilibrium PDEs for an accurate recovery of stress components in thin-walled rectangular and circular cross-sections.

Finally, non vanishing shear stress induced by pure bending loads introduces a further feature that needs to be addressed: the non-prismatic beam constitutive relations. Indeed, if the shear stress distribution explicitly depends on the bending moments, it is reasonable to expect that also shear deformation depends on bending moment, leading to conclude that prismatic beam constitutive relations with variable coefficients are simplistic. The problem has been identified since the end of the past century [70, 58]. Nevertheless, effective strategies for the evaluation of non-prismatic beam constitutive relations have been proposed only in recent years. Balduzzi et al. [9] have achieved the goal, embedding the information coming from non-prismatic beam stress recovery in the stress potential and computing simple derivative, while Rajagopal [53] has obtained similar constitutive relations using the variational asymptotic method.

Summarizing, the following three features have to be considered for the development of effective models and accurate analysis tools for non-prismatic beams.

I. **Variable stiffness.** Variations of the cross-section thickness lead the ODEs analytical solution to be non-polynomial, even for linearly tapered beams, and not available for arbitrarily complicated geometries [65, 57, 56].
II. **Non-trivial shear stress.** The equilibrium BC leads the shear-stress to be proportional to the axial

stress on lateral surfaces [20, 70, 21, 34, 35]. As a consequence, the shear stress does not uniquely depend on the transversal internal force, rather also on axial internal force and bending moment [64, 24, 66, 10].

III. **Complicated constitutive relations.** Similarly to shear stress, also the shear deformation depends on all internal forces, requiring the use of more complicated constitutive relations [15, 9, 7].

Considering the problem from practitioners' perspective, the above mentioned features prove that analytical and numerical tools developed for prismatic beams (e.g., FEs, stress recovery procedures, simplified estimations of the maximal stress) are not adequate for the structural analysis and the design of non-prismatic beams. Conversely, commercial software, design standards, and handbooks often ignore these problems, coarsely estimating quantities of interest for practitioners [73] and, in extreme situations, leading to wrong estimation of the real structural element resistance [10, 16, 47].

To the best of authors' knowledge, few contributions simultaneously tackle all the three features above mentioned. An attempt in this direction was proposed by Auricchio et al. [6] that use high order kinematics and highly refined stress distribution. The obtained model is extremely accurate, nevertheless its complexity leads to a set of ODEs which require numerical tools to be solved, even in the simplest cases. According to these encouraging results, Beltempo et al. [15] used a similar derivation procedure, but adopted a Timoshenko-like kinematics (i.e., assuming that the cross-section behaves as a rigid body) and simplified hypotheses on stress distributions. The obtained model is simpler than the one proposed by Auricchio et al. [6], showing a similar accuracy. Later on, Balduzzi et al. [9] derive a non-prismatic beam model that uses Timoshenko kinematic parameters and internal forces as independent Degree Of Freedoms (DOFs). The simplicity of the resulting ODEs allows the explicit calculation both for homogeneous and particular solutions. Anyway, analytical results can be computed and handled only for extremely simple geometries and load distributions, restricting the practical utility of such an analytical result. Finally, a beam model similar to [9] was obtained also by Rajagopal [53] using the variational asymptotic method.

1.2. Numerical discretization

Moving from the continuous 1D modeling to the numerical discretization of non-prismatic beams, the discussion can focus on FE-like methods whose fundamental components are the element stiffness matrices that are defined according to the nodal unknowns (usually displacements) and the corresponding shape functions. Features of continuous 1D models, discussed in Section 1.1, do not allow for an immediate numerical discretization of the non-prismatic beams, leading to an extensive literature in this specific field, as discussed in the following.

The simplest numerical approach for solving non-prismatic beam models is the so-called stepped beam approximation. It consists of approximating the non-prismatic beam as a sequence of prismatic elements [38, 55, 49]. Obviously, such an approach converges to some solution, but it needs a lot of elements to achieve a reasonable accuracy due to Feature I. - variable stiffness. Furthermore, it overlooks Features II. - non-trivial shear stress and III. - complicated constitutive relations, turning out to be inconsistent and uselessly expensive. Nevertheless, the above mentioned modeling approach is suggested in standard FE literature [79, Chapter 1], lecture notes, and several commercial FE software tutorials.

A slightly more refined strategy consists of numerical solution of suitable weak formulations of the non-prismatic beam model. As an example, Just [37] used the Euler Bernoulli beam theory and the virtual work principle to compute the stiffness matrix terms, considering modified shape functions to account for variations in cross-section area and second moment of area. Aiming at reducing the computational cost, Browns [23] proposed a method where approximated interpolation functions were used to obtain bending stiffness matrix. Another option was proposed in [78, Chapter 10] in which mixed formulations of both Euler Bernoulli and Timoshenko beams are exploited in order to increase the accuracy of the obtained numerical solution.

Eisenberger [27] derived stiffness matrix for structural elements with variable cross-section considering the flexibility method. Another approach, based on flexibility method and Timoshenko theory, was presented by Tena-Colunga [62], who included shear deformation and the variability of the cross-section for both 2D and 3D non-prismatic beams.

Murin and Kutiš [45] used the direct stiffness method and transfer functions in order to evaluate the FE stiffness matrix of a 3D beam with continuous variation of the cross-section area. More recently, Zhi-Luo et al. [76] exploited the transfer matrix method for evaluating the stiffness matrix of both continuous and discontinuous non-prismatic structural elements. Using the same method, Gimena et al. [31, 32] studied spatial arch models providing both analytical results and numerical approximate procedures for curved beams with different support conditions. Finally, Shooshtari and Khajavi [60] analyzed shape functions and stiffness matrices of non-prismatic beams using a similar procedure.

Failla and Impollonia [29] developed a method based on the theory of generalized functions to solve non-uniform and discontinuous beams in static analysis, resulting particularly useful in sensitivity, damage identification, and optimization. Trinh and Gan [67] derived shape functions for a linearly tapered Timoshenko solid beam element starting from the Hamilton principle. Finally, Tudjono et al. [68] explicitly derived "exact" shape functions for both non-prismatic section and non-homogeneous Timoshenko beam elements.

Unfortunately, all the above-mentioned researches treat Feature I. - variable stiffness, but neglect either Feature II. - non-trivial shear stress or Feature III. - complicated constitutive relations, undermining the accuracy of all the proposed numerical tools.

El-Mezaini et al. [28] studied the behavior of stepped and haunch planar beams by means of 2D FE analysis. More recently, Balkaya [13] studied the behavior of beams whose cross section thickens toward its supports and having T-section, estimating the stiffness of an equivalent two-node beam element with fictitious average second moment of area and area by means of a 3D FE analysis. Such a strategy properly addresses all non-prismatic beam features, but (i) it is extremely expensive from the computational point of view, (ii) it does not allow an easy recovery of displacements and stresses, and (iii) it impedes the explicitly identification of non-prismatic beam features and a deep understanding of the behavior of non-prismatic structural elements.

Due to the difficulties connected with the correct modeling of non-prismatic beams, most of commercial software started to include tapered elements in their libraries only from the early 2000s. Since then, the use of commercial software in the analysis of non-prismatic structural elements diffused worldwide among practitioners. Also in the research field, some authors use commercial software to validate their models. As an example, Zeinali et al. [75] use results obtained using SAP2000 [25] as reference solution for the discussion of the accuracy of the method they proposed.

Tena-Colunga and Becerril [63] investigated the accuracy of structural analysis commercial software evaluating how accurate are ETABS and STAAD-Pro solutions when RC haunch beam are modeled. The scrupulous and extensive parametric study shows that both ETABS and STAAD-Pro generally provide reasonable estimations, but it leads to an underestimation of both the lateral displacements and bending moments. Anyway, the stiffness coefficients taken from [62] are considered as reference values and the study is limited to the analysis of the global stiffness of structures using non-prismatic structural-elements, while it does not properly address Feature II. - non-trivial shear stress, lacking information on the strength.

2. 2D non-prismatic beam model derivations

This section derives analytical NPBMs. Subsection 2.1 defines the beam geometry and formulates the 2D problem. Subsection 2.2 introduces the displacement approximation and derives analytical expressions for stress recovery. Finally, Subsections 2.3 and 2.4 derive the full and the simplified NPBMs, respectively.

If compared to the non-prismatic beam model proposed by Beltempo et al. [15], the NPBMs discussed in the following (i) increases the model physical soundness, thanks to the use of internal forces as independent variables, (ii) improves the description of stress distribution, and (iii) simplifies the resulting ODEs, allowing for an effective handling of the beam analytical solution.

2.1. Problem formulation

As illustrated in Figure 1, the region $\Omega \subset \mathbb{R}^2$ occupied by the planar beam is defined introducing a closed and bounded set $[0, L]$ of the x axis, the beam centerline i.e., a continuously differentiable function $c(x)$, and

the cross-section thickness i.e., a strictly positive definite and continuously differentiable function $t(x) > 0$. For convenience, we assume that

$$1 \gg |c'(x)| \gg t(x)\,|c''(x)| \;\text{ and }\; 1 \gg |t'(x)| \gg t(x)\,|t''(x)| \tag{1}$$

where the notation $(\,\cdot\,)'$ denotes the derivative with respect to x. The beam lower and upper bounds $h_l(x)$ and $h_u(x)$ are defined as

$$h_l(x) = c(x) - \frac{t(x)}{2}; \qquad h_u(x) = c(x) + \frac{t(x)}{2} \tag{2}$$

A peculiar property of the above mentioned geometry description is that the cross-section is perpendicular to the x axis. Such a modeling choice is substantially different from standard modeling approach used for curved beams where the cross-section is assumed to be perpendicular to the centerline [2, Chapter IV], [33]. However, as discussed in [54], such an exotic choice may have advantages in several situations. Certainly, it allows to bypass the need of parametric definition of the beam centerline and the use of additional local coordinate systems, with the associated coordinate transformations and derivative chains.

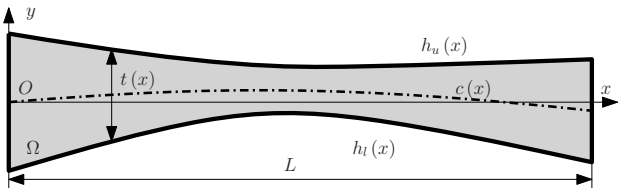

Figure 1: Geometric parameters of the generic non-prismatic beam.

The beam has a constant depth b along the z direction and it behaves under the assumption of plane stress and small displacements. The material constituting the beam is linear-elastic and isotropic, its constitutive law is defined by the Young's modulus E and the Poisson's coefficient ν, and the shear modulus G reads

$$G = \frac{E}{2\,(1+\nu)} \tag{3}$$

The planar linear elastic problem is represented by the following set of 2D PDEs

$$\boldsymbol{\epsilon}(x,y) = \nabla^s \boldsymbol{s}(x,y) \qquad \text{in } \Omega \tag{4a}$$
$$\nabla \cdot \boldsymbol{\sigma}(x,y) = -\,\boldsymbol{f}(x,y) \qquad \text{in } \Omega \tag{4b}$$
$$\boldsymbol{\epsilon}(x,y) = \boldsymbol{D} : \boldsymbol{\sigma}(x,y) \qquad \text{in } \Omega \tag{4c}$$
$$\boldsymbol{s}(x,y) = \boldsymbol{0} \qquad \text{in } \partial\Omega_s \tag{4d}$$
$$\boldsymbol{\sigma}(x,y) \cdot \boldsymbol{n}(x,y) = -\,\boldsymbol{g}(x,y) \qquad \text{in } \partial\Omega_g \tag{4e}$$

where

- $\boldsymbol{s}(x,y)$ is the 2D displacement field,
- $\boldsymbol{\epsilon}(x,y)$ and $\boldsymbol{\sigma}(x,y)$ are the planar strain and stress tensors, respectively,
- $\nabla^s(\,\cdot\,)$ and $\nabla\cdot\,(\,\cdot\,)$ are the symmetric gradient and the divergence operators, respectively,
- $\boldsymbol{f}(x,y)$ and $\boldsymbol{g}(x,y)$ are the distributed and the boundary loads, respectively,
- $\partial\Omega_s$ and $\partial\Omega_g$ are the displacement constrained and loaded boundaries, respectively,
- $\boldsymbol{D}$ the fourth order tensor representing the linear elastic isotropic material constitutive law, and
- $\boldsymbol{n}(x,y)$ is the normal unit vector.

The derivation of the NPBM starts from a variational formulation of the 2D linear elastic problem. Specifically, we consider the mixed Hellinger-Reissner functional where only the displacement $\boldsymbol{s}(x,y)$ and

the stress $\boldsymbol{\sigma}(x,y)$ are the unknown fields, leading to the following expression.

$$\begin{aligned} &\text{Find } \boldsymbol{s} \text{ and } \boldsymbol{\sigma} \text{ such that } \forall \delta\boldsymbol{s} \text{ and } \forall \delta\boldsymbol{\sigma} \\ &\int_{\Omega} \left(\delta\boldsymbol{s}\cdot\nabla\cdot\boldsymbol{\sigma} + \nabla\cdot\delta\boldsymbol{\sigma}\cdot\boldsymbol{s} + \delta\boldsymbol{\sigma}:\boldsymbol{D}:\boldsymbol{\sigma} + \delta\boldsymbol{s}\cdot\boldsymbol{f}\right) d\Omega = 0 \end{aligned} \tag{5}$$

where the boundary equilibrium (4e) is an essential condition, directly enforced on stress field, while displacement constrain (4d) is a natural one. Readers are recommended to refer to [15, Section 2.2] and [4] for a more detailed discussion of the problem formulation.

We assume that the upper and lower bounds are unloaded (i.e., $h_u(x)$ and $h_l(x) \in \partial\Omega_g$ and $\boldsymbol{g}(x,y)|_{h_{u,l}} = \mathbf{0}$), while the beam has some displacement constraint on the initial or final cross-sections in order to guarantee the well-posedness of the problem i.e., avoiding rigid-body motions.

2.2. Approximation of displacement and stress distributions

Suitable approximations of both displacement and stress cross-section distributions have to be introduced, in order to reduce the 2D problem (5) defined on Ω into a 1D problem defined on $[0, L]$.

The displacement components $s_x(x,y)$ and $s_y(x,y)$ are assumed in the following form

$$\left\{\begin{array}{c} s_x(x,y) \\ s_y(x,y) \end{array}\right\} \approx \left[\begin{array}{ccc} 1 & 0 & c(x)-y \\ 0 & 1 & 0 \end{array}\right] \left\{\begin{array}{c} u(x) \\ v(x) \\ \theta(x) \end{array}\right\} \tag{6}$$

where $u(x)$, $v(x)$, and $\theta(x)$ represent the horizontal displacement, the vertical displacement, and the rotation of the cross-section, respectively.

The stress components $\sigma_x(x,y)$, $\sigma_y(x,y)$, and $\tau(x,y)$ are assumed in the following form

$$\left\{\begin{array}{c} \sigma_x(x,y) \\ \sigma_y(x,y) \\ \tau(x,y) \end{array}\right\} \approx \left[\begin{array}{ccc} d^H_{\sigma_x}(x,y) & 0 & d^M_{\sigma_x}(x,y) \\ d^H_{\sigma_y}(x,y) & d^V_{\sigma_y}(x,y) & d^M_{\sigma_y}(x,y) \\ d^H_{\tau}(x,y) & d^V_{\tau}(x,y) & d^M_{\tau}(x,y) \end{array}\right] \left\{\begin{array}{c} H(x) \\ V(x) \\ M(x) \end{array}\right\} \tag{7}$$

where $H(x)$, $V(x)$, and $M(x)$ represent the horizontal force, the vertical force, and the bending moment resulting from the stress acting on the cross-section, respectively. For convenience of representation, the following functions have been used

$$d^H_{\sigma_x}(x,y) = \frac{1}{tb} \tag{8a}$$

$$d^M_{\sigma_x}(x,y) = \frac{12(c-y)}{t^3 b} \tag{8b}$$

$$\begin{aligned} d^H_{\sigma_y}(x,y) =& 2\frac{6c't' - tc''}{t^4 b}y^3 + \frac{12c'^2t - 36ct'c' + tt'^2 + 6c''tc - \frac{t^2t''}{2}}{t^4 b}y^2 + \\ & \frac{\left(-12c^2t + t^3\right)c'' + 2\left(t''\right)ct^2 - 48c'^2ct + \left(72c^2 - 2t^2\right)t'c' - 4t'^2ct}{2t^4 b}y + \\ & \frac{\left(4c^3t - ct^3\right)c'' + \left(\frac{t^4}{4} - c^2t^2\right)t'' - 4\left(\left(6c^2 - t^2\right)c' - \frac{ctt'}{2}\right)\left(t'c - c't\right)}{2t^4 b} \end{aligned} \tag{8c}$$

$$\begin{aligned} d^M_{\sigma_y}(x,y) =& 6\frac{t''t - 4t'^2}{t^5 b}y^3 + 6\frac{12t'^2c - 3t''ct + c''t^2 - 6c't't}{t^5 b}y^2 + \\ & 3\frac{6c^2tt'' - 24c^2t'^2 - 4ct^2c'' + 24ctc't' - \frac{1}{2}t^3t'' - 4t^2c'^2 + t^2t'^2}{t^5 b}y + \\ & \frac{\left(12c^2t^2 - 3t^4\right)c'' + 3ct\left(t^2 - 4c^2\right)t'' + 24\left(\left(2c^2 - \frac{t^2}{4}\right)t' - tc'c\right)\left(t'c - tc'\right)}{2t^5 b} \end{aligned} \tag{8d}$$

$$d^V_{\sigma_y}(x,y) = -\frac{12t'}{t^4 b}y^3 + 12\frac{3t'c - tc'}{t^4 b}y^2 + 3\frac{t^2t' - 12c^2t' + 8tc'c}{t^4 b}y + 3\frac{\left(4c^2 - t^2\right)\left(t'c - tc'\right)}{t^4 b} \tag{8e}$$

$$d^H_{\tau}(x,y) = \frac{6c'}{t^3 b}y^2 + \frac{t't - 12cc'}{t^3 b}y + \frac{6c^2c'}{t^3 b} - \frac{t'c}{t^2 b} - \frac{c'}{2tb} \tag{8f}$$

$$d^M_{\tau}(x,y) = -\frac{18t'}{t^4 b}y^2 + \frac{36t'c - 12c't}{t^4 b}y + \frac{12c'c}{t^3 b} - \frac{18t'c^2}{t^4 b} + \frac{3t'}{2t^2 b} \tag{8g}$$

$$d^V_{\tau}(x,y) = -\frac{6}{t^3 b}y^2 - \frac{12c}{t^3 b}y - \frac{6c^2}{t^3 b} + \frac{3}{2tb} \tag{8h}$$

where the explicit dependence of the functions c and t on the axial coordinate x has been omitted for notation compactness.

Stress distributions (8) have been obtained using a procedure similar to the one discussed in [26, 50] and considering equilibrium boundary conditions detailed in [15, 7]. As a consequence, stress distribution (7) satisfies (i) equilibrium PDEs (4b) and (ii) the boundary equilibrium (4e) at beam lower and upper bounds. Conversely, Beltempo et al. [15] just interpolate the transversal stresses evaluated at upper and lower bounds by means of boundary equilibrium. As a consequence, the cubic distribution of transversal stress (7) turns out being more accurate than the stress description provided in [15], [9, 7] (where transversal stress has been neglected), and [42, 41] (where transversal stress has a parabolic distribution).

A further advantage of the proposed stress representation with respect to the modeling approach proposed in [15] is that in Equation (7) the stress distribution explicitly depends on the resulting internal forces, allowing for a more easy interpretation of the model. Furthermore, Equation (7) clearly shows that $\tau(x,y)$ depends on both axial internal force $H(x)$ and bending moment $M(x)$, effectively solving Feature II. - non-trivial shear stress.

Finally, considering a prismatic beam (i.e., assuming $c(x) = 0$ and $t(x) = t_0$), the non-vanishing stress distributions (8) reduces to

$$d^H_{\sigma_x}(x,y) = \frac{1}{t_0 b}; \quad d^M_{\sigma_x}(x,y) = -\frac{12y}{t_0^3 b}; \quad d^V_{\tau}(x,y) = -\frac{3\left(t_0^2 - 4y^2\right)}{2t_0^3 b} \tag{9}$$

i.e., to the standard distribution of stresses in prismatic beams.

Since the proposed beam model formulation allows the use of cross-sections non-orthogonal to the centerline, a discussion of the effects of this feature on the model effectiveness has to be provided. As discussed in [64, Section 35], a parabolic distribution of shear stress is a good approximation of the analytical solution of equilibrium PDEs in infinite long wedge. Consistently, Auricchio et al. [6] have shown that a parabolic distribution of shear and a cubic distribution of transversal stresses leads to extremely accurate description of stresses in non-prismatic beams. Conversely, no information is available for a prismatic beam with inclined centerline.

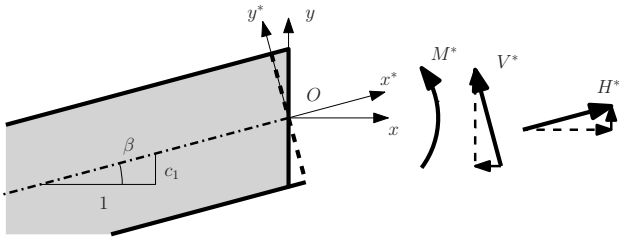

Figure 2: Prismatic beam with inclined centerline, Cartesian coordinate systems, and applied loads.

Considering the prismatic beam ($t(x) = t_0$) with inclined centerline ($c(x) = c_1 x$) depicted in Figure 2, the stress tensor $\boldsymbol{\sigma}^*$ represented in the Cartesian coordinate system Ox^*y^* reads

$$\boldsymbol{\sigma}^*(x^*,y^*) = \begin{bmatrix} \sigma_x^*(x^*,y^*) & \tau^*(x^*,y^*) \\ \tau^*(x^*,y^*) & \sigma_y^*(x^*,y^*) \end{bmatrix} = \boldsymbol{R}^T \begin{bmatrix} \sigma_x(x,y) & \tau(x,y) \\ \tau(x,y) & \sigma_y(x,y) \end{bmatrix} \boldsymbol{R} \tag{10}$$

where $[x^*, y^*]^T = \boldsymbol{R}\,[x, y]^T$, the stress tensor components σ_x, τ, and σ_y are defined according to Equation (7), the matrix $\boldsymbol{R}$ reads

$$\boldsymbol{R} = \begin{bmatrix} \cos(\beta) & -\sin(\beta) \\ \sin(\beta) & \cos(\beta) \end{bmatrix} \tag{11}$$

and the notation $(\cdot)^T$ denotes the transposition operation. Exploiting hypothesis (1), we can assume that $\beta \approx \sin(\beta) \approx \tan(\beta) = c_1$. Accordingly, the stress distribution evaluated within the cross-section orthogonal to the beam centerline (the dashed line in Figure 2) reads

$$\boldsymbol{\sigma}^*(0, y^*) = \begin{bmatrix} 1 & c_1 \\ -c_1 & 1 \end{bmatrix} \begin{bmatrix} \sigma_x(-c_1 y, y) & \tau(-c_1 y, y) \\ \tau(-c_1 y, y) & \sigma_y(-c_1 y, y) \end{bmatrix} \begin{bmatrix} 1 & -c_1 \\ c_1 & 1 \end{bmatrix} \tag{12}$$

Considering $M^*(0) = 1$ as the only acting internal force, the stress distributions evaluated according to Equation (7) read

$$\begin{aligned} \sigma_x(x, y) &= d^M_{\sigma_x}(x, y) = -\frac{12y}{t_0^3 b} \\ \tau(x, y) &= d^M_{\tau}(x, y) = -\frac{12c_1 y}{t_0^3 b} \\ \sigma_y(x, y) &= d^M_{\sigma_y}(x, y) = -\frac{12c_1^2 y}{t_0^3 b} \end{aligned} \tag{13}$$

Applying transformation (12), the stress components σ_x^*, σ_y^*, and τ^* read

$$\sigma_x^*(0, y^*) = -\frac{12y^*}{t_0^3 b}\left(1 + o\left(c_1^2\right)\right); \quad \tau^*(0, y^*) = 0; \quad \sigma_y^*(0, y^*) = 0 \tag{14}$$

In a similar way, considering an axial force $H^*(0) = 1$ parallel to the beam centerline (i.e., $H(0) = 1$ and $V(0) = c_1$) leads to the following distribution of stresses

$$\begin{aligned} \sigma_x(x, y) &= d^H_{\sigma_x}(x, y) = \frac{1}{t_0 b} \\ \tau(x, y) &= d^H_{\tau}(x, y) + c_1 d^V_{\tau}(x, y) = \frac{c_1}{t_0 b} \\ \sigma_y(x, y) &= d^H_{\sigma_y}(x, y) + c_1 d^V_{\sigma_y}(x, y) = \frac{c_1^2}{t_0 b} \end{aligned} \tag{15}$$

Applying transformation (12), the stress components σ_x^*, σ_y^*, and τ^* read

$$\sigma_x^*(0, y^*) = \frac{1}{t_0 b}\left(1 + o\left(c_1^2\right)\right); \quad \tau^*(0, y^*) = 0; \quad \sigma_y^*(0, y^*) = 0 \tag{16}$$

Finally, considering a transversal force $V^*(0) = 1$ perpendicular to the beam centerline (i.e., $H(0) = -c_1$, $V(0) = 1$, and $M(x) = -c_1 y$) leads to the following distribution of stresses

$$\begin{aligned} \sigma_x(x, y) &= -c_1 d^H_{\sigma_x}(x, y) - c_1 y d^M_{\sigma_x}(x, y) = c_1\left(\frac{12y^2}{t_0^3 b} - \frac{1}{t_0 b}\right) \\ \tau(x, y) &= -c_1 d^H_{\tau}(x, y) - c_1 y d^M_{\tau}(x, y) + d^V_{\tau}(x, y) = \frac{3\left(t_0^2 - 4y^2\right)}{2t_0^3 b} + o\left(c_1^2\right) \\ \sigma_y(x, y) &= -c_1 d^H_{\sigma_y}(x, y) - c_1 y d^M_{\sigma_y}(x, y) + d^V_{\sigma_y}(x, y) = c_1\left(\frac{12y^2}{t_0^3 b} - \frac{1}{t_0 b}\right) + o\left(c_1^3\right) \end{aligned} \tag{17}$$

Applying transformation (12), the stress components σ_x^*, σ_y^*, and τ^* reads

$$\sigma_x^*(0, y^*) = o(c_1); \quad \tau^*(0, y^*) = \frac{3\left(t_0^2 - 4y^{*2}\right)}{2t_0^3 b} + o\left(c_1^2\right); \quad \sigma_y^*(0, y^*) = 0 \tag{18}$$

Neglecting high order terms, Equations (14), (16), and (18) are identical to Equation (9), demonstrating that stress recovery (7) leads to a stress distribution that coincides with the one for prismatic beam, for small values of the centerline slope. This proves that the considered modeling approach leads to stress distribution consistent with standard beam results, confirming the effectiveness of the modeling strategy, at least under the considered hypothesis. Further comments on the accuracy of the proposed stress recovery can be found in Section 3, where numerical examples will be considered.

2.3. Derivation of full NPBM ODEs

We substitute Equations (6) and (7) in the 2D functional (5), we analytically evaluate integrals within the cross-section, and, finally, we integrate by parts terms in which x derivative is applied to virtual fields. Requiring to satisfy the resulting weak problem for all admissible virtual fields leads to the following ODEs

$$\begin{Bmatrix} H' \\ V' \\ M' \\ u' \\ v' \\ \theta' \end{Bmatrix} = \begin{bmatrix} 0 & 0 & 0 & & & \\ 0 & 0 & 0 & & \mathbf{0} & \\ H_{MN} & H_{MV} & 0 & & & \\ H_{uH} & H_{uV} & H_{uM} & 0 & 0 & H_{u\theta} \\ H_{vH} & H_{vV} & H_{vM} & 0 & 0 & H_{v\theta} \\ H_{\theta H} & H_{\theta M} & H_{\theta V} & 0 & 0 & 0 \end{bmatrix} \begin{Bmatrix} H \\ V \\ M \\ u \\ v \\ \theta \end{Bmatrix} - \begin{Bmatrix} q \\ p \\ m \\ 0 \\ 0 \\ 0 \end{Bmatrix} \tag{19}$$

Also in Equation (19), dependencies on the beam axis variable x were omitted for notation simplicity and the matrix terms read

$$H_{MN} = -H_{u\theta} = c' \tag{20a}$$

$$H_{MV} = -H_{v\theta} = -1 \tag{20b}$$

$$\begin{aligned} H_{uH} = &\frac{1}{420tbE}\left(2t^2c'^2 + 4tc't'c'' + 7\frac{t^2t''^2}{2} - 7\left(14c'^2t - \frac{t}{2}\left(t'^2 - 20\nu\right)\right)t''\right. \\ &\left. +756c'^4 + 30\left(t'^2 + 28\nu\right)c'^2 + 7\left(\frac{3}{4}t'^4 - 10\nu t'^2 + 60\right)\right) + \frac{10t'^2 + 24c'^2}{120tbG} \end{aligned} \tag{20c}$$

$$H_{uM} = H_{\theta H} = \frac{42t\left(c'^2 - \frac{t'^2}{28} - \frac{2t''t}{21} + \nu\right)c'' + 3tc't't'' - 112t'c'^3 - 4\left(3t'^3 - 7t'\nu\right)c'}{35t^2bE} - \frac{8t'c'}{5t^2bG} \tag{20d}$$

$$H_{uV} = H_{vH} = \frac{2t't^2c'' + 14c't^2t'' - 196tc'^3 + \left(9tt'^2 - 140t\nu\right)c'}{70t^2bE} - \frac{c'}{5tbG} \tag{20e}$$

$$\begin{aligned} H_{\theta M} = &\frac{3}{5t^3bE}\left(2t^2c'^2 - 4tc't'c'' + \frac{t^2t''^2}{14} + 2t\left(-\frac{t'^2}{28} + c'^2 - \nu\right)t'' + \frac{11}{28}t'^4\right. \\ &\left. +2\left(7c'^2 - \nu\right)t'^2 + 20c'^4 - 40\nu c'^2 + 20\right) + \frac{63t'^2 + 420c'^2}{35t^3bG} \end{aligned} \tag{20f}$$

$$H_{\theta V} = H_{vM} = 3\frac{tt'^3 - 56t^2c''c' - 2t^2t''t' + 28t\left(c'^2 + \nu\right)t'}{70t^3bE} + \frac{3t'}{5t^2bG} \tag{20g}$$

$$H_{vV} = 6\frac{t'^2t + 28c'^2t}{35t^2bE} + \frac{6}{5tbG} \tag{20h}$$

$$q = \int_{h_l(x)}^{h_u(x)} f_x\left(x, y\right) dy \tag{20i}$$

$$p = \int_{h_l(x)}^{h_u(x)} f_y\left(x, y\right) dy \tag{20j}$$

$$m = \int_{h_l(x)}^{h_u(x)} f_x\left(x, y\right)\left(c\left(x\right) - y\right) dy \tag{20k}$$

In ODEs (19), all matrix coefficients H_{iJ} with $i = u, \theta, v$ and $J = H, M, V$ do not vanish. Furthermore, all of them depend on both material mechanical properties and cross-section geometry, indicating that NPBM overcomes Feature III. - complicated constitutive relations.

2.4. Derivation of simplified NPBM

ODEs (19) have been derived on the basis of enhanced stress recovery (7). However, the coefficients (20c)-(20h) can be simplified exploiting the hypothesis (1) that allows to neglect second derivatives and squared (or higher order) first derivatives. This leads to the formulation of the following simplified model

$$\begin{Bmatrix} \tilde{H}' \\ \tilde{V}' \\ \tilde{M}' \\ \tilde{u}' \\ \tilde{v}' \\ \tilde{\theta}' \end{Bmatrix} = \begin{bmatrix} 0 & 0 & 0 & & & \\ 0 & 0 & 0 & & \mathbf{0} & \\ \tilde{H}_{MN} & \tilde{H}_{MV} & 0 & & & \\ \tilde{H}_{uH} & \tilde{H}_{uV} & 0 & 0 & 0 & \tilde{H}_{u\theta} \\ \tilde{H}_{vH} & \tilde{H}_{vV} & \tilde{H}_{vM} & 0 & 0 & \tilde{H}_{v\theta} \\ 0 & \tilde{H}_{\theta M} & \tilde{H}_{\theta V} & 0 & 0 & 0 \end{bmatrix} \begin{Bmatrix} \tilde{H} \\ \tilde{V} \\ \tilde{M} \\ \tilde{u} \\ \tilde{v} \\ \tilde{\theta} \end{Bmatrix} - \begin{Bmatrix} q \\ p \\ m \\ 0 \\ 0 \\ 0 \end{Bmatrix} \tag{21}$$

in which the notation $\tilde{(\cdot)}$ has been used in order to distinguish coefficients and solution of the simplified model. The coefficients $\tilde{H}_{ij}$ read

$$\tilde{H}_{MN} = -H_{u\theta} = c' \tag{22a}$$

$$\tilde{H}_{MV} = -H_{v\theta} = -1 \tag{22b}$$

$$\tilde{H}_{uH} = \frac{1}{tbE} \tag{22c}$$

$$\tilde{H}_{uV} = \tilde{H}_{vH} = -\frac{c'}{5tbG} - \frac{2c'\nu}{tbE} \tag{22d}$$

$$\tilde{H}_{\theta M} = \frac{1}{12t^3bE} \tag{22e}$$

$$\tilde{H}_{\theta V} = \tilde{H}_{vM} = \frac{6\nu t'}{5t^2bE} + \frac{3t'}{5t^2bG} \tag{22f}$$

$$\tilde{H}_{vV} = \frac{6}{5tbG} \tag{22g}$$

Equations (22c), (22e), and (22g), excluding the dependence of t, c and their derivatives on x, coincide with stiffness coefficients of prismatic beams. Conversely, Equations (22d) and (22f) point out that constitutive relations for non-prismatic beams are more complex than the ones of prismatic beams not just for the variability of cross-section area and second moment of area. Specifically, shear force is associated to non-vanishing bending moment and beam horizontal deformation.

Finally, the stiffness coefficients $\tilde{H}_{uV}$ and $\tilde{H}_{\theta V}$ (Equations (22d) and (22f)) explicitly depend on the Poisson's coefficient ν. These terms appear because we considered also the transversal stress σ_y, indicating that it influences the whole structural behavior and, as a consequence, it cannot be neglected (as usual in standard prismatic beam).

3. Numerical validation of the proposed NPBMs

This section discusses two numerical examples, aiming at verifying the accuracy of NPBMs derived in Section 2. More in details, we consider numerical examples proposed in [15] and compare also different models available in literature. We consider a depth $b = 1$ m, while the material has the following mechanical properties

$$E = 10^5 \text{ MPa}; \qquad \nu = 0.3 \tag{23}$$

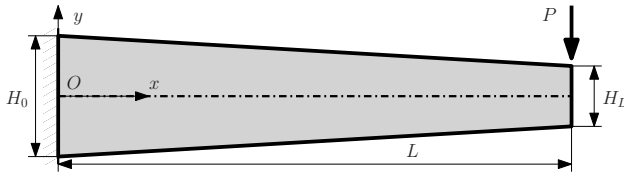

Figure 3: Tapered symmetric cantilever loaded by a vertical concentrated force. $L = 10$ m, $H_0 = 1$ m, $H_L = 0.5$ m, $P = 100$ kN.

3.1. Tapered symmetric cantilever

This subsection considers the tapered cantilever depicted in Figure 3, loaded on the right hand side cross-section with a concentrated vertical force $P = 100$ kN.

The reference solution for the problem introduced above has been constructed using the FE software Abaqus [61] and it has been obtained discretizing the 2D beam domain Ω with a structured mesh of 2000×150 CPS4 (4-node bi-linear plane-stress) FEs. The characteristic element size (0.005 m) has been chosen in order to guarantee negligible numerical errors in the Abaqus solution. Aiming at mitigating the influence of local effects induced by the constraint in left hand side cross-section and the load distribution in right hand side cross-section, a distributing coupling constraint has been created, using the points $(0, 0)$ and $(0, L)$ as reference nodes and a uniform weighting method. Cross-section displacements have been evaluated by means of appropriate average / interpolation of nodal displacements, following a procedure similar to the one detailed in [12, Section 5].

Considering a generic variable ψ, the relative error is defined as

$$e_\psi = 100 \frac{|\psi - \psi_{ref}|}{|\psi_{ref}|} \tag{24}$$

where ψ_{ref} is the reference value of the variable evaluated according to 2D FE analysis introduced above.

Table 1 reports the maximum vertical displacement $v(L)$ and rotation $\theta(L)$ evaluated according to different beam models. Full NPBM and the model proposed by Beltempo et al. [15] show the best accuracy

model	$v(L)$ [mm]	e_v [%]	$\theta(L)$ [mrad]	e_θ [%]
Euler-Bernoulli	-6.5421	$5.28 \cdot 10^{-1}$	-1.2000	$6.67 \cdot 10^{-2}$
Timoshenko	-6.5854	$1.31 \cdot 10^{-1}$	-1.2000	$6.67 \cdot 10^{-2}$
Beltempo et al [15]	-6.577	$3.04 \cdot 10^{-3}$	-	-
simp. NPBM Eq. (21)	-6.5705	$9.58 \cdot 10^{-2}$	-1.1981	$9.17 \cdot 10^{-2}$
full NPBM Eq. (19)	-6.5764	$6.08 \cdot 10^{-3}$	-1.1992	$1.67 \cdot 10^{-2}$
ψ_{ref} (2D FE)	-6.5768	-	-1.1994	-

Table 1: Evaluation of tapered cantilever maximal displacements, comparison of different beam models.

in estimating the vertical displacement. As expected, simplified NPBM is less accurate, estimating vertical displacement with an error close to 0.1 %. Finally, standard Euler-Bernoulli and Timoshenko beams with variable cross-section stiffness are the coarse models, with relative errors up to 0.5 %.

Figure 4 depicts the distribution of shear and transversal stresses evaluated at $x = 5$ m according to different beam models. As already noticed by Beltempo et al. [15], Timoshenko beam stress recovery is not effective for tapered beams. Both NPBM and the model proposed by Beltempo et al. [15] provide a more accurate description of the shear stress distribution. More in details, Figure 4(a) allows to recognize the contribution of bending moment to the shear stress distribution, justifying the apparently paradoxical constant distribution of shear within the cross-section.

The post-processing procedure in commercial software SAP2000 [25] estimates shear stress only in points (cross-section centroid and boundaries) that may be critical for the cross-section design. It is evident that provided estimations of the shear stress are consistent with prismatic Timoshenko beam theory and therefore, not reliable for the structural analysis of tapered beams.

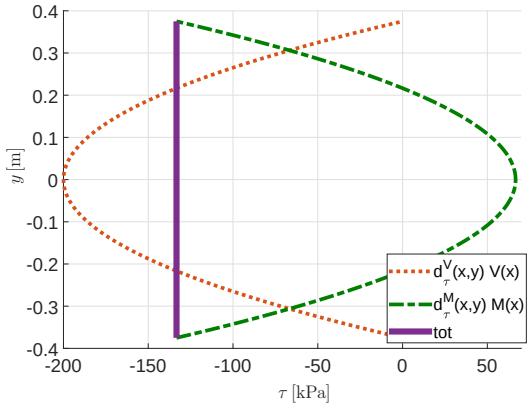

(a) Shear stress components $\tau\,(5, y)$

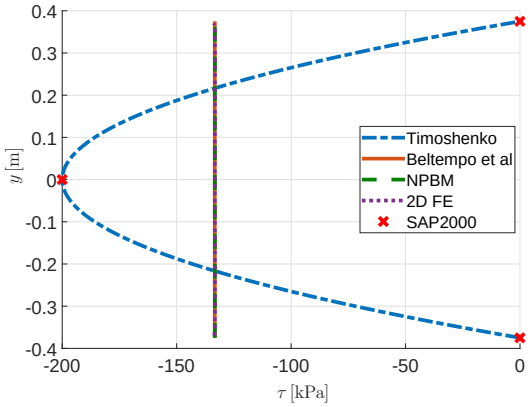

(b) Shear stress $\tau\,(5, y)$

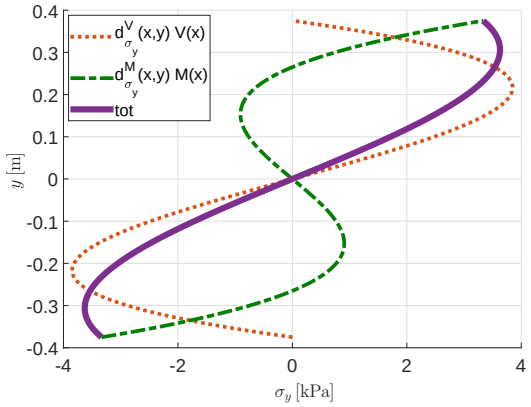

(c) Transversal stress components $\sigma_y\,(5, y)$

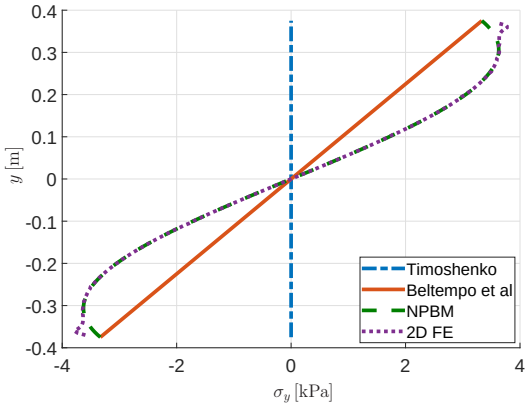

(d) Transversal stress $\sigma_y\,(5, y)$

Figure 4: Tapered cantilever, distribution of shear and transversal stresses evaluated at $x = 5$ m. Comparison of different models.

Concerning the recovery of transversal stress, Figure 4(d) highlights that NPBMs provide an accurate estimation of this quantity, while Beltempo et al. [15] provides coarser estimations, with relative errors larger than 30%. Finally, Timoshenko beam model assumes that this stress component has a vanishing magnitude and no information on this stress component is provided in SAP2000 post processing routines.

Transversal stress is two order of magnitude smaller than shear stress, hence it can be neglected for isotropic materials, like steel. However, transversal stress tends to concentrate near the cross-section boundaries, where also axial stress and shear are large in magnitude. As a consequence, transversal stress can play a crucial role for materials with reduced (or vanishing) resistance to traction, like concrete for which a beam model capable to accurately estimate such a quantity may be extremely useful during structural design.

3.2. Non-symmetric parabolic-shaped cantilever

This subsection considers the non-symmetric parabolic-shaped cantilever depicted in Figure 5, loaded on the right hand side cross-section with a concentrated vertical force $P = 100$ kN and a horizontal force $Q = 100$ kN. Beltempo et al. [15] have analyzed the same beam considering the vertical and the horizontal loads separately. Considering only the horizontal load, numerical results point out that the maximal vertical displacement is three times larger than the horizontal one. The huge influence of the beam centerline on the beam stiffness was previously noticed by Auricchio et al. [6] analyzing an arch shaped beam subjected

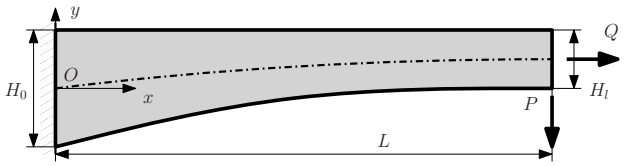

Figure 5: Non-symmetric parabolic-shaped cantilever loaded by a generic concentrated force. $L = 5$ m, $H_0 = 1$ m, $H_L = 0.5$ m, $P = Q = 100$ kN.

to an axial load and, more recently, by Murin et al. [44] in the context of enhanced FGM beam modeling. The reference solution for the problem introduced above has been obtained using a procedure similar to the one described in Section 3.1 and a structured mesh of 1000×100 elements.

Table 2 reports the maximum displacements $u(L)$, $v(L)$, and rotation $\theta(L)$ evaluated according to different beam models. Timoshenko beam model leads to the coarsest estimation, with relative error larger

model	$u(L)$ [mm]	e_u [%]	$v(L)$ [mm]	e_v [%]	$\theta(L)$ [mrad]	e_θ [%]
Timoshenko	$7.8540 \cdot 10^{-6}$	$8.32 \cdot 10^{1}$	$-1.2026 \cdot 10^{-3}$	$3.89 \cdot 10^{0}$	$-4.5001 \cdot 10^{-4}$	$3.40 \cdot 10^{0}$
Beltempo et al [15]	-	-	$-1.2138 \cdot 10^{-2}$	$3.00 \cdot 10^{0}$	-	-
simp. NPBM Eq. (21)	$4.6892 \cdot 10^{-5}$	$6.19 \cdot 10^{-2}$	$-1.2293 \cdot 10^{-3}$	$1.76 \cdot 10^{0}$	$-4.5987 \cdot 10^{-4}$	$1.28 \cdot 10^{0}$
full NPBM Eq. (19)	$4.6939 \cdot 10^{-5}$	$1.62 \cdot 10^{-1}$	$-1.2471 \cdot 10^{-3}$	$3.36 \cdot 10^{-1}$	$-4.6473 \cdot 10^{-4}$	$2.38 \cdot 10^{-1}$
ψ_{ref} (2D FE)	$4.6863 \cdot 10^{-5}$	-	$-1.2513 \cdot 10^{-3}$	-	$-4.6584 \cdot 10^{-4}$	-

Table 2: Evaluation of parabolic-shaped cantilever maximal displacements, comparison of different beam models.

than 3 % for all the three considered quantities. The model proposed by Beltempo et al. [15] provides a better estimation, but the error is anyway near to 3 %. Conversely, the simplified NPBM leads to errors below 2 %, while the full NPBM provides the best estimation of maximal displacements, with errors below 0.5 %.

Figure 6 depicts the distribution of shear and transversal stresses evaluated at $x = 2.5$ m according to different beam models. Figure 6(b) clearly shows that, also in this case, shear recovery formula associated to Timoshenko beam leads to unreliable results. The maximal magnitude of shear stress is underestimated more than 35 %. Furthermore, Timoshenko beam model assumes a-priori that maximal shear stress occurs at the cross-section centroid, while -in reality- maximal shear stress occurs at the cross-section lower bound. Conversely, the shear stress recovery procedure proposed by Beltempo et al. [15] and the one derived in this paper lead to a more reliable estimation of the distribution of shear stress, with relative errors smaller than 3 %. Figure 6(a) explains why the shear stress occurs at the cross-section lower bound where the shear is proportional to the magnitude of axial stress. In the specific case, bending moment produces the main effects, while axial load is negligible.

Figure 6(d) confirms that the transversal stress recovery proposed in this document is effective even for non-trivial geometries and with arbitrary load conditions. NPBM estimates the distribution of transversal stresses with negligible errors, while Beltempo et al. [15] leads to errors larger than 30 %. Similarly to shear stress distribution, Figure 6(c) illustrates the non-negligible effects that axial internal force and bending moment have on the distribution of transversal stress.

3.3. Conclusion on analytical beam models

Numerical results illustrated in Section 3 demonstrate that standard analytical beam models and commerical FE software developed for prismatic beams do not reliably describe the behavior of non-prismatic beams. Indeed they lead to coarse estimation of displacements (with errors larger than 3 % for statically determinate structures) and stresses (with errors larger than 30 % in the estimation of shear and equal to 100 % for transversal stress). The model proposed by Beltempo et al. [15] is more accurate, however it just linearly interpolates the distribution of transversal stresses, leading to errors larger than 30 %. Finally NPBMs provide the best accuracy in the recovery of stress distribution, with errors usually below 3 %.

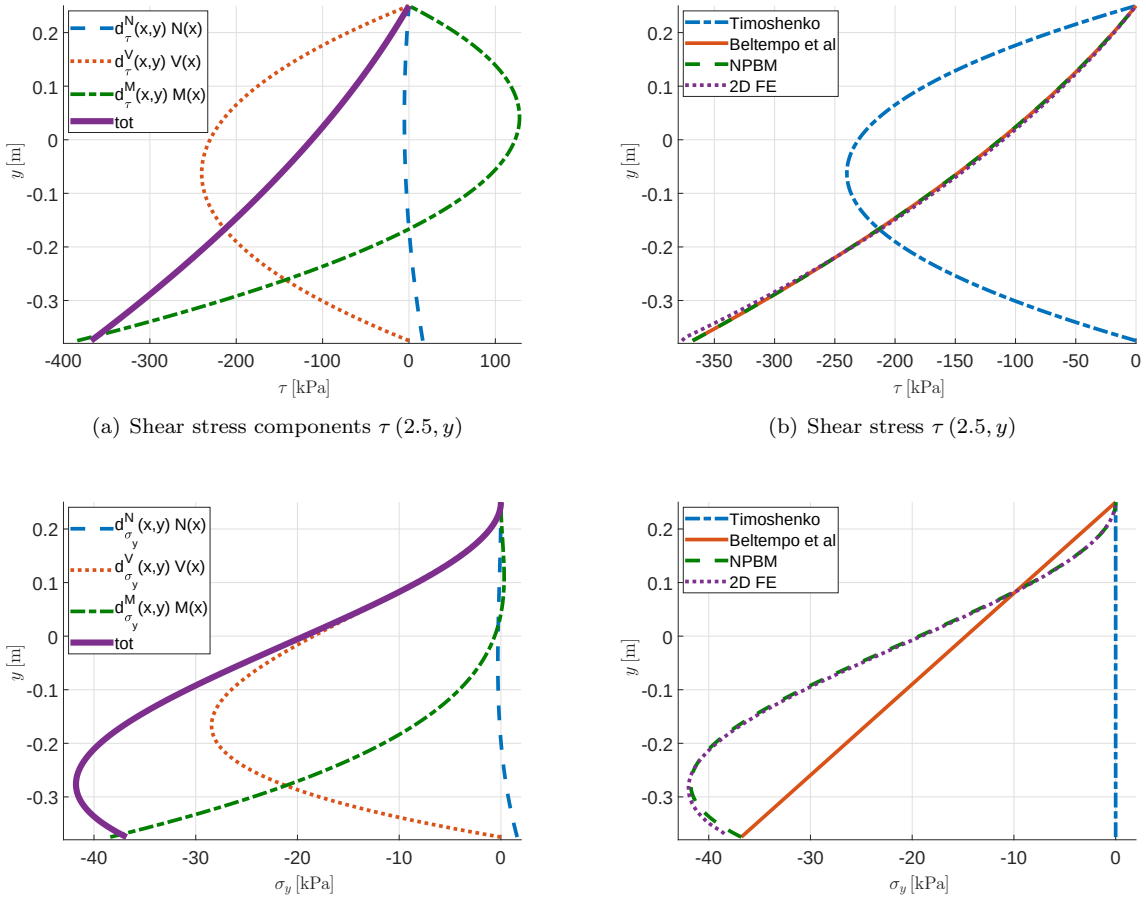

(a) Shear stress components $\tau\,(2.5, y)$

(b) Shear stress $\tau\,(2.5, y)$

(c) Transversal stress components $\sigma_y\,(2.5, y)$

(d) Transversal stress $\sigma_y\,(2.5, y)$

Figure 6: Parabolic-shaped cantilever, distribution of shear and transversal stresses evaluated at $x = 2.5$ m. Comparison of different models.

The full NPBM leads also to extremely accurate estimations of displacements, with errors usually below 0.5 %, but the complexity of the equations does not allow an easy handling of the analytical solution. Conversely, the simplified NPBM has a lower accuracy in the estimations of displacements, with errors below 2 % (sufficient for most of practical applications), but its handling is simpler.

4. Analytical definition of tapered beam FE stiffness matrix

This section evaluates FE stiffness matrix using the beam model developed in Section 2. Considering the linearly-tapered symmetric beam depicted in Figure 7(a) (i.e., assuming $c\,(x) = 0$ and $t\,(x) = t_0 + t_1 x$) leads ODEs (21) to further simplify, as follows

$$\begin{Bmatrix} \tilde{H}' \\ \tilde{V}' \\ \tilde{M}' \\ \tilde{u}' \\ \tilde{v}' \\ \tilde{\theta}' \end{Bmatrix} = \begin{bmatrix} 0 & 0 & 0 & & & \\ 0 & 0 & 0 & & \mathbf{0} & \\ 0 & \tilde{H}_{MV} & 0 & & & \\ \tilde{H}_{uH} & 0 & 0 & 0 & 0 & 0 \\ 0 & \tilde{H}_{vV} & \tilde{H}_{vM} & 0 & 0 & \tilde{H}_{v\theta} \\ 0 & \tilde{H}_{\theta M} & \tilde{H}_{\theta V} & 0 & 0 & 0 \end{bmatrix} \begin{Bmatrix} \tilde{H} \\ \tilde{V} \\ \tilde{M} \\ \tilde{u} \\ \tilde{v} \\ \tilde{\theta} \end{Bmatrix} - \begin{Bmatrix} q \\ p \\ m \\ 0 \\ 0 \\ 0 \end{Bmatrix} \tag{25}$$

More in details, the axial problem, depending on variables $\tilde{H}$ and $\tilde{u}$, decouples from the shear bending problem depending on $\tilde{V}$, $\tilde{M}$, $\tilde{v}$, and $\tilde{\theta}$ due to the symmetry of the geometry.

The homogeneous solution associated to ODEs (25) reads

$$\tilde{H} = C_6 \tag{26a}$$

$$\tilde{V} = C_5 \tag{26b}$$

$$\tilde{M} = -C_5 x + C_3 \tag{26c}$$

$$\tilde{u} = C_4 + \frac{\ln\left(t_1 x + t_0\right) C_6}{E t_1 b} \tag{26d}$$

$$\begin{aligned}\tilde{v} = &\frac{6}{Eb}\left(\frac{2C_5 \ln\left(t_1 x + t_0\right)}{{t_1}^3} + \frac{C_3 t_1 + t_0 C_5}{\left(t_1 x + t_0\right){t_1}^3}\right) - \frac{\nu}{Eb}\left(\frac{12 C_5 \ln\left(t_1 x + t_0\right)}{5 t_1} + \frac{6 C_3 t_1 + 6 t_0 C_5}{5 t_1 \left(t_1 x + t_0\right)}\right) \\ &- \frac{3 C_3 t_1 + 3 t_0 C_5}{5 t_1 \left(t_1 x + t_0\right) G b} + C_2 x + C_1\end{aligned} \tag{26e}$$

$$\tilde{\theta} = \frac{\left(12 C_5 x - 6 C_3\right) t_1 + 6 t_0 C_5}{E b {t_1}^2 \left(t_1 x + t_0\right)^2} + -\frac{6 \nu C_5}{5\left(t_1 x + t_0\right) E b} - \frac{3 C_5}{5 G b \left(t_1 x + t_0\right)} + C_2 \tag{26f}$$

The particular solution for ODEs (25) obtained considering a uniformly distributed transversal load p and a uniformly distributed axial load q reads

$$\tilde{H} = q x \tag{27a}$$

$$\tilde{V} = p x \tag{27b}$$

$$\tilde{M} = -1/2 p x^2 \tag{27c}$$

$$\tilde{u} = \frac{-\ln\left(t_1 x + t_0\right) q t_0 + q x t_1}{{t_1}^2 E b} \tag{27d}$$

$$\begin{aligned}\tilde{v} = &-\frac{6p}{{t_1}^4 E b}\left(\left(t_1 x + 3 t_0\right)\ln\left(t_1 x + t_0\right) - \frac{2{t_1}^2 x^2 + 4 t_0 t_1 x + {t_0}^2}{2\left(t_1 x + t_0\right)}\right) \\ &+ \frac{6 \nu p}{5 E b {t_1}^2}\left(\left(t_1 x + 3 t_0\right)\ln\left(t_1 x + t_0\right) - \frac{3{t_1}^2 x^2 + 6 t_0 t_1 x + 2{t_0}^2}{2\left(t_1 x + t_0\right)}\right) \\ &+ \frac{3p}{5{t_1}^2 G b}\left(\left(t_1 x + t_0\right)\ln\left(t_1 x + t_0\right) + \frac{{t_1}^2 x^2 + 2 t_0 t_1 x + 2{t_0}^2}{2\left(t_1 x + t_0\right)}\right)\end{aligned} \tag{27e}$$

$$\tilde{\theta} = -\frac{6p}{E b {t_1}^3}\left(\ln\left(t_1 x + t_0\right) + \frac{4 t_0 t_1 x + 3{t_0}^2}{2\left(t_1 x + t_0\right)^2}\right) + \left(\frac{6 \nu p}{5 E b t_1} + \frac{3p}{5 G b t_1}\right)\left(\ln\left(t_1 x + t_0\right) + \frac{t_0}{\left(t_1 x + t_0\right)}\right) \tag{27f}$$

Both homogeneous and particular solutions of ODEs (25) were computed using the symbolic-calculus software MAPLE [40], overcoming any possible issue coming from Feature I. - variable stiffness.

Exploiting the analogy between direct stiffness and FE methods [30], the stiffness matrix and the load vector for a generic tapered beam were analytically computed assuming appropriate BCs and loads. Specifically, the i^{th} column of the beam stiffness matrix was calculated assigning vanishing loads and a unitary value to the i^{th} nodal displacement. Stiffness matrix coefficients are the resulting internal forces at beam extremities. Similarly, load vector is computed evaluating the resulting internal forces at beam extremities, considering vanishing nodal displacements and suitable load distributions.

Stiffness matrix coefficients are associated to the set of nodal DOFs and sign convention reported in

Figure 7(b), reducing ODEs (19) to the following algebraic problem

$$\begin{bmatrix} K_{11} & 0 & 0 & K_{14} & 0 & 0 \\ 0 & K_{22} & K_{23} & 0 & K_{25} & K_{26} \\ 0 & K_{32} & K_{33} & 0 & K_{35} & K_{36} \\ K_{41} & 0 & 0 & K_{44} & 0 & 0 \\ 0 & K_{52} & K_{53} & 0 & K_{55} & K_{56} \\ 0 & K_{62} & K_{63} & 0 & K_{65} & K_{66} \end{bmatrix} \begin{Bmatrix} \hat{u}_1 \\ \hat{v}_1 \\ \hat{\theta}_1 \\ \hat{u}_2 \\ \hat{v}_2 \\ \hat{\theta}_2 \end{Bmatrix} = \begin{Bmatrix} \hat{H}_1 \\ \hat{V}_1 \\ \hat{M}_1 \\ \hat{H}_2 \\ \hat{V}_2 \\ \hat{M}_2 \end{Bmatrix} \tag{28}$$

where

$$K_{11} = \frac{Ebt_1}{\ln(Lt_1 + t_0) - \ln(t_0)} \tag{29a}$$

$$\begin{aligned} K_{22} = &-50EG^2 b {t_1}^3 (Lt_1 + 2t_0) / \left(120G^2 \left(\nu {t_1}^2 - 5\right)(Lt_1 + 2t_0)\ln(Lt_1 + t_0)\right. \\ &\left.-120G^2 \left(\nu {t_1}^2 - 5\right)(Lt_1 + 2t_0)\ln(t_0) + 3\left((2G\nu + E){t_1}^2 - 20G\right)^2 t_1 L\right) \end{aligned} \tag{29b}$$

$$\begin{aligned} K_{23} = &5t_0 Gb\left(L(2G\nu + E){t_1}^2 + t_0(2G\nu + E)t_1 - 10GL\right) E{t_1}^3 / \\ &\left(120G^2\left(\nu {t_1}^2 - 5\right)(Lt_1 + 2t_0)\ln(Lt_1 + t_0) - 120G^2\left(\nu {t_1}^2 - 5\right)(Lt_1 + 2t_0)\ln(t_0)\right. \\ &\left.+3\left((2G\nu + E){t_1}^2 - 20G\right)^2 t_1 L\right) \end{aligned} \tag{29c}$$

$$\begin{aligned} K_{33} = &-10{t_0}^2 GEb\left(-2G(Lt_1 + t_0)^2\left(\nu {t_1}^2 - 5\right)\ln(Lt_1 + t_0) + 2G(Lt_1 + t_0)^2\left(\nu {t_1}^2 - 5\right)\ln(t_0)\right. \\ &\left.+\left(\left(2L\nu {t_1}^3 + 2\nu t_0 {t_1}^2 - 15Lt_1 - 10t_0\right)G + E{t_1}^2(Lt_1 + t_0)\right)t_1 L\right) / \\ &3L / \left(40G^2\left(\nu {t_1}^2 - 5\right)(Lt_1 + 2t_0)\ln(Lt_1 + t_0) - 40G^2\left(\nu {t_1}^2 - 5\right)(Lt_1 + 2t_0)\ln(t_0) + \right. \\ &\left.\left(\left(2\nu {t_1}^2 - 20\right)G + E{t_1}^2\right)^2 t_1 L\right) \end{aligned} \tag{29d}$$

$$K_{14} = K_{41} = -K_{44} = -K_{11} \tag{29e}$$

$$K_{25} = K_{52} = -K_{55} = -K_{22} \tag{29f}$$

$$K_{32} = -K_{35} = -K_{53} = K_{23} \tag{29g}$$

$$K_{26} = K_{62} = -K_{56} = -K_{65} = K_{22}L - K_{23} \tag{29h}$$

$$K_{36} = K_{63} = K_{23}L - K_{33} \tag{29i}$$

$$K_{66} = (K_{22}L - K_{23})L - K_{23}L + K_{33} \tag{29j}$$

$$\hat{H}_1 = \frac{q\left(Lt_1 - \ln(Lt_1 + t_0)t_0 + t_0\ln(t_0)\right)}{t_1\left(-\ln(Lt_1 + t_0) + \ln(t_0)\right)} \tag{30a}$$

$$\begin{aligned} \hat{V}_1 = &p\left(-\left(L(2G\nu + E)^2 {t_1}^5 + t_0(2G\nu + E)^2 {t_1}^4 - 10(10G\nu + 3E)GL{t_1}^3 - 10Gt_0(14G\nu + 3E){t_1}^2\right.\right. \\ &\left.+400G^2 Lt_1 + 600G^2 t_0\right)t_0\ln(Lt_1 + t_0) + \left(L(2G\nu + E)^2 {t_1}^5 + t_0(2G\nu + E)^2 {t_1}^4\right. \\ &-30(10/3G\nu + E)GL{t_1}^3 - 10Gt_0(14G\nu + 3E){t_1}^2 + 400G^2 Lt_1 + 600G^2 t_0\Big)t_0\ln(t_0) \\ &+t_1\left(t_0(2G\nu + E)^2 {t_1}^4 + 5GL(-6G\nu + E){t_1}^3 - 30Gt_0(14/3G\nu + E){t_1}^2 + 100G^2 Lt_1\right. \\ &\left.\left.+600G^2 t_0\right)L\right) / \left(t_1\left(40G^2\left(\nu {t_1}^2 - 5\right)(Lt_1 + 2t_0)\ln(Lt_1 + t_0)\right.\right. \\ &\left.\left.-40G^2\left(\nu {t_1}^2 - 5\right)(Lt_1 + 2t_0)\ln(t_0) + t_1\left((2G\nu + E){t_1}^2 - 20G\right)^2 L\right)\right) \end{aligned} \tag{30b}$$

$$
\begin{aligned}
\hat{M}_1 =& t_0 p \Big(8 \left(\nu {t_1}^2 - 5\right) G \left(\left(2G\nu + E\right) {t_1}^2 - 10G \right) \left(Lt_1 + t_0\right)^2 t_0 \left(\ln\left(Lt_1 + t_0\right)\right)^2 \\
& -2t_0 \Big(8 \left(\nu {t_1}^2 - 5\right) G \left(\left(2G\nu + E\right) {t_1}^2 - 10G \right) \left(Lt_1 + t_0\right)^2 \ln\left(t_0\right) + t_1 \Big(L \left(2G\nu + E\right)^2 {t_1}^5 \\
& + t_0 \left(2G\nu + E\right)^2 {t_1}^4 - 10 \left(8G\nu + 3E\right) GL{t_1}^3 - 10 \left(10G\nu + 3E\right) Gt_0 {t_1}^2 + 300G^2 L t_1 \\
& + 400G^2 t_0 \Big) L \Big) \ln\left(Lt_1 + t_0\right) + 8 \left(\nu {t_1}^2 - 5\right) G \left(\left(2G\nu + E\right) {t_1}^2 - 10G \right) \left(Lt_1 + t_0\right)^2 t_0 \left(\ln\left(t_0\right)\right)^2 \\
& + 2t_1 \Big(L \left(2G\nu + E\right)^2 {t_1}^5 + t_0 \left(2G\nu + E\right)^2 {t_1}^4 - 30 \left(8/3G\nu + E\right) GL{t_1}^3 - 10 \left(10/G\nu + 3E\right) Gt_0 {t_1}^2 \\
& + 300G^2 L t_1 + 400G^2 t_0 \Big) t_0 L \ln\left(t_0\right) + {t_1}^2 \Big(L \left(2G\nu + E\right) \left(-6G\nu + E\right) {t_1}^5 + \left(-8G^2\nu^2 t_0 + 2E^2 t_0\right) {t_1}^4 \\
& + 10GL \left(10G\nu + E\right) {t_1}^3 - 20Gt_0 \left(2G\nu + E\right) {t_1}^2 - 200G^2 L t_1 + 400G^2 t_0 \Big) L^2 \Big) / \\
& \Big(-2{t_1}^3 \left(40G^2 \left(\nu {t_1}^2 - 5\right) \left(Lt_1 + 2t_0\right) \ln\left(Lt_1 + t_0\right) - 40G^2 \left(\nu {t_1}^2 - 5\right) \left(Lt_1 + 2t_0\right) \ln\left(t_0\right) \right. \\
& \left. + t_1 \left(\left(2G\nu + E\right) {t_1}^2 - 20G \right)^2 L \Big) L \Big)
\end{aligned}
\tag{30c}
$$

$$
\hat{H}_2 = qL - \hat{H}_1 \tag{30d}
$$

$$
\hat{V}_2 = pL - \hat{V}_1 \tag{30e}
$$

$$
\hat{M}_2 = \hat{M}_1 - \hat{V}_2 L + \frac{qL^2}{2} \tag{30f}
$$

Evaluating coefficients (29) and (30) for $t_1 = 0$ (i.e., considering a prismatic beam) leads to indeterminate forms 0/0. However, evaluating their limits for $t_1 \to 0$ the following values are obtained

$$
\lim_{t_1 \to 0} K_{11} = \frac{Et_0 b}{L} \tag{31a}
$$

$$
\lim_{t_1 \to 0} K_{22} = 5 \frac{GEb{t_0}^3}{6EL{t_0}^2 + 5GL^3} \tag{31b}
$$

$$
\lim_{t_1 \to 0} K_{23} = 5 \frac{GEb{t_0}^3}{12E{t_0}^2 + 10GL^2} \tag{31c}
$$

$$
\lim_{t_1 \to 0} K_{33} = \frac{3{t_0}^5 E^2 b + 10EGbL^2 {t_0}^3}{36EL{t_0}^2 + 30GL^3} \tag{31d}
$$

$$
\lim_{t_1 \to 0} \hat{H}_1 = \frac{1}{2} Lq; \quad \lim_{t_1 \to 0} \hat{V}_1 = \frac{1}{2} Lp; \quad \lim_{t_1 \to 0} \hat{M}_1 = \frac{1}{12} L^2 p \tag{32}
$$

The stiffness coefficients and the nodal load vector obtained for prismatic beam according to the model proposed in this paper are identical to the ones reported in standard literature [78], confirming the capability of NPBM to recover trivial solutions.

5. Numerical validation of the proposed tapered beam FE stiffness matrix

This section discusses the accuracy of the modeling approach presented in Section 4 in the evaluation of the stiffness matrix of an elementary linearly-tapered beam. Accordingly, the FE stiffness matrices of several linearly tapered beams have been evaluated using analytical formulas (29) and the commercial software SAP2000, while the reference solution has been computed using 2D FE and the commercial software Abaqus.

According to SAP2000 Analysis Reference Manual [25], cross-sections are defined independently and then assigned to the element. Variations of cross-section geometry along the element length is accounted referring to previously defined cross-section geometries and interpolating the values assigned at the two ends. Furthermore, users can choose the interpolation to be used for bending stiffness which can be linear, quadratic, or cubic, suggesting to use linear interpolation for beams having linearly-varying depth, quadratic

interpolation for thin walled beams with variable thickness, and cubic interpolation for rectangular cross-sections with variable thickness. Regarding the remaining properties (axial and shear stiffness, mass and weight), they are assumed to vary linearly between the ends of each FE. The user may also specify length l of segments to be used for the analysis of non-prismatic beams. Using this option allows to reduce the magnitude of numerical errors, nevertheless this straightforward technique of dividing a tapered beam into a number of uniform elements is scarcely efficient [75]. Cubic interpolation for the bending stiffness in vertical plane and other default settings (relative length $l = 0.5$, linear interpolation for the bending stiffness in horizontal plane) are used and each tapered beam has been modeled with a single beam FE.

Abaqus solution is obtained using the approach introduced in Section 3.1. The clamp of initial and final cross-sections has been modeled constraining all DOFs of reference nodes $(0, 0)$ and $(0, L)$. The i^{th} column of the beam stiffness matrix has been calculated assigning a unitary value to the i^{th} reference node displacement and evaluating the reaction forces.

5.1. Parametric study

The parametric study presented in this section considers a symmetric tapered beam, as in Figure 7. To study NPBM and SAP2000 accuracy, the obtained results have been compared with those calculated with the FE software Abaqus.

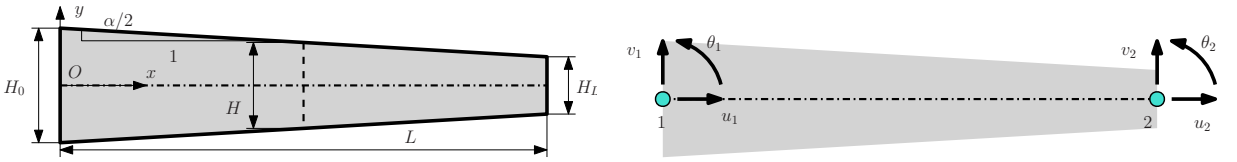

(a) Symmetric tapered beam

(b) DOFs definition

Figure 7: Symmetric tapered beam geometry considered for the parametric study and definition of nodal DOFs and sign convention adopted for the coefficients of the stiffness matrix.

More in details, we define the taper $\alpha = |H_L - H_0| / L$, where H_0 and H_L are the heights evaluated for $x = 0$ and $x = L$, respectively. We consider $0 \leq \alpha \leq 0.2$, $L/H = 10, 5, 2.5$, where $H = (H_0 + H_L)/2 = 1$m, and we set the beam depth $b = 1$ m. The mechanical properties of the material are defined in Equation (23).

The average error of the stiffness matrix is defined as

$$err_K = \frac{\sum_{i,j=1..6} \left| K_{ij}^{mod} - K_{ij}^{ABQ} \right|}{\sum_{i,j=1..6} \left| K_{ij}^{ABQ} \right|} \tag{33}$$

with $mod = NPM$, SAP and K_{ij}^{ABQ} is the reference value, evaluated using Abaqus.

Figure 8 plots the NPBM and SAP2000 errors err_K as a function of the taper α for different beam slenderness. Considering $\alpha = 0$, the stiffness matrix error increases, decreasing the beam slenderness. Such a behavior is expected since the accuracy of the beam model increases with the beam slenderness, as well documented in literature (see [5] and therein referenced papers). In a similar way, given a fixed beam slenderness L/H, the stiffness matrix error increases increasing the beam taper α. Also this behavior is expected and well documented in literature. Timoshenko and Goodier [64] discussing the stress distribution within an infinite long wedge specified that a parabolic distribution of shear stress is a reasonable approximation of the analytical solution for small taper. Obviously, also the accuracy of the model decreases for increasing taper and the numerical results are consistent with the above discussed theoretical argumentation.

Comparing the performances of different modeling approaches, it is evident that NPBM leads to an estimation of the stiffness matrix that is similar or better than the estimation provided by SAP2000 in most of cases. Specifically, NPBM and SAP2000 perform very similarly for ratios $L/H = 10, 5$, while SAP2000 leads to an error on the stiffness matrix evaluation that is more than 1.5 times larger than the error of NPBM for $L/H = 2.5$ and $\alpha = 0.2$. Finally, NPBM errors are always smaller than 0.9 %, while SAP2000 errors overcome the threshold of 1.2 %.

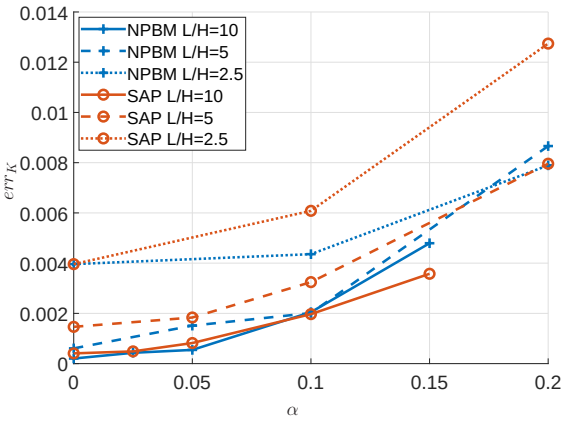

Figure 8: NPBM and SAP2000 stiffness matrix error evaluated for varying taper α nd beam slenderness L/H.

5.2. Explicit stiffness matrix

This section reports the stiffness matrix coefficients for a tapered beam obtained respectively with Abaqus ($\boldsymbol{K}^{ABQ}$), the NPBM ($\boldsymbol{K}^{NPBM}$), and SAP2000 ($\boldsymbol{K}^{SAP}$). This explicit comparison aims at discussing more in detail differences between the NPBM and SAP2000 stiffness matrices.

Considering $\alpha = 0.2$ and $L/H = 2.5$ we obtain

$$\boldsymbol{K}^{ABQ} = 10^7 \cdot \begin{bmatrix} 3.880 & & & & & \\ 0 & 0.417 & & & sym & \\ 0 & 0.661 & 1.338 & & & \\ -3.880 & 0 & 0 & 3.880 & & \\ 0 & -0.417 & -0.661 & 0 & 0.417 & \\ 0 & 0.381 & 0.315 & 0 & -0.381 & 0.637 \end{bmatrix} \tag{34}$$

$$\boldsymbol{K}^{NPBM} = 10^7 \cdot \begin{bmatrix} 3.915 & & & & & \\ (0.91) & & & & & \\ 0 & 0.417 & & & sym & \\ & (0.12) & & & & \\ 0 & 0.664 & 1.351 & & & \\ & (0.51) & (0.99) & & & \\ -3.915 & 0 & 0 & 3.915 & & \\ (0.91) & & & (0.91) & & \\ 0 & -0.417 & -0.664 & 0 & 0.417 & \\ & (0.12) & (0.51) & & (0.12) & \\ 0 & 0.379 & 0.310 & 0 & -0.379 & 0.637 \\ & (0.55) & (1.52) & & (0.55) & (0.07) \end{bmatrix} \tag{35}$$

$$\boldsymbol{K}^{SAP} = 10^7 \cdot \begin{bmatrix} 3.915 & & & & & \\ (0.91) & & & & & \\ 0 & 0.413 & & & sym & \\ & (0.86) & & & & \\ 0 & 0.646 & 1.302 & & & \\ & (2.35) & (2.71) & & & \\ -3.915 & 0 & 0 & 3.915 & & \\ (0.91) & & & (0.91) & & \\ 0 & -0.413 & -0.646 & 0 & 0.413 & \\ & (0.86) & (2.35) & & (0.86) & \\ 0 & 0.387 & 0.312 & 0 & -0.387 & 0.656 \\ & (1.73) & (0.83) & & (1.73) & (2.99) \end{bmatrix} \tag{36}$$

In Equations (35) and (36), the numbers in parenthesis are the differences with the reference values expressed in percentage $100 \left| K_{ij}^{mod} - K_{ij}^{ABQ} \right| / \left| K_{ij}^{ABQ} \right|$.

The axial stiffness terms (K_{ij} for $i, j = 1, 4$) evaluated with both NPBM and SAP2000 are identical and in good agreement with the reference stiffness matrix $\boldsymbol{K}^{ABQ}$, just leading to a small overestimation (< 1 %) of the beam stiffness. This result is expected since in simplified NPBM axial and shear-bending problems are decoupled (see Equation (25))and the axial stiffness (22c) is equivalent to the prismatic beam stiffness, just accounting for the linear variation of cross-section area and consistently with the SAP2000 interpolation.

The situation is different for the shear bending problem, for which SAP2000 overestimates the stiffness matrix coefficients with errors often larger than 2 %, while analytical expressions (29) lead to estimations associated to errors always below 1 %. Such a simple remark confirms critical issues in SAP2000 already noticed by Tena-Colunga and Becerril [63] for other FE commercial software.

6. Final remarks

This paper proposes effective strategies for the analytical and numerical modeling of non-prismatic beams. The literature review highlights that the analysis of structures with non-prismatic elements are characterized by three features: (I) **variable stiffness**, leading to non-polynomial solution of the beam model ODEs, (II) **non-trivial shear stress**, depending on both bending and axial loads, and (III) **complicated constitutive relations**.

Aiming at overcoming these critical issues, the present paper proposes two -full and simplified- non-prismatic planar beam models and exploits the simplified NPBM analytical solution for the computation of tapered element stiffness matrix. Aiming at evaluating the performances of existing modeling strategies, we carried out a parametric study on single element stiffness matrix. We considered (i) the FE proposed in this paper, (ii) the numerical results of the commercial software SAP2000, and (iii) a 2D FE analysis done using Abaqus (used as reference solution).

Results highlight that SAP2000 estimates structural element stiffness with errors larger than 2 % and maximal magnitude of shear stress with errors up 30 %. Furthermore, SAP2000 does not correctly predict the location of the maximal shear stress and it does not provides information about transversal stress. Conversely, NPBM based FE estimates stiffness with errors usually smaller than 1 % and maximal magnitude of stress components with errors usually below 3 %. NPBM-based FE achieves also the best numerical performance since (i) it does not need any pre-processing and post-processing computation, (ii) it uses standard nodal DOFs and (iii) it allows to model one structural component with just one FE.

Commercial software results confirm that non-prismatic beams need ad-hoc analysis tools, not yet available for practitioners. Conversely, NPBM-based FE allows for a a consistent and effective modeling of non-prismatic beams, representing a promising base for the development of enhanced and reliable analysis tools for non-prismatic beams.

Further developments of the present work will include the exploitation of full NPBM model, aiming at further increasing the accuracy of the proposed method, the generalization of the NPBM to 3D frames, and

the implementation of numerical approaches considering reinforcing bars effects and non-linear constitutive relations.

Acknowledgments

F. Auricchio and V. Mercuri acknowledge that the present study falls under the framework of the 3D@ UniPV project (http://www.unipv.it/3d), a strategic research areas of the University of Pavia.

References

[1] Al-Ghatani, H. and M. Khan (1998). Exact analysis of nonprismatic beams. *Journal of Engineering Mechanics 124*, 1290–1293.

[2] Antman, S. (2013). *Nonlinear Problems of Elasticity*. Applied Mathematical Sciences. Springer New York.

[3] Asprone, D., F. Auricchio, C. Menna, and V. Mercuri (2018). 3d printing of reinforced concrete elements: Technology and design approach. *Construction and Building Materials 165*, 218–231.

[4] Auricchio, F., G. Balduzzi, and C. Lovadina (2010). A new modeling approach for planar beams: Finite-element solutions based on mixed variational derivations. *Journal of Mechanic of Materials and Structures 5*, 771–794.

[5] Auricchio, F., G. Balduzzi, and C. Lovadina (2013). The dimensional reduction modelling approach for 3D beams: Differential equations and finite-element solutions based on hellinger-reissner principle. *International Journal of Solids and Structures 50*, 4184–4196.

[6] Auricchio, F., G. Balduzzi, and C. Lovadina (2015). The dimensional reduction approach for 2D non-prismatic beam modelling: a solution based on Hellinger-Reissner principle. *International Journal of Solids and Structures 15*, 264–276.

[7] Balduzzi, G., M. Aminbaghai, F. Auricchio, and J. Füssl (2017). Planar Timoshenko-like model for multilayer non-prismatic beams. *International Journal of Mechanics and Materials in Design* -(-), 1–20.

[8] Balduzzi, G., M. Aminbaghai, and J. Füssl (2017). Linear response of a planar FGM beam with non-linear variation of the mechanical properties. In A. Güemes, A. Benjeddou, J. Rodellar, and J. Leng (Eds.), *SMART 2017*, pp. 1285–1294. CIMNE.

[9] Balduzzi, G., M. Aminbaghai, E. Sacco, J. Füssl, J. Eberhardsteiner, and F. Auricchio (2016). Non-prismatic beams: a simple and effective Timoshenko-like model. *International Journal of Solids and Structures 90*, 236–250.

[10] Balduzzi, G., G. Hochreiner, and J. Füssl (2017). Stress recovery from one dimensional models for tapered bi-symmetric thin-walled I beams: deficiencies in modern engineering tools and procedures. *Thin walled structures 119*, 934–944.

[11] Balduzzi, G., G. Hochreiner, J. Füssl, and F. Auricchio (2016). Performance evaluation of new straightforward formulas for the serviceability analysis of cambered timber beams. In *Proceedings of the Word Conference on Timber Engineering*.

[12] Balduzzi, G., S. Morganti, J. Füssl, M. Aminbaghai, A. Reali, and F. Auricchio (2019). Modeling the non-trivial behavior of anisotropic beams: A simple Timoshenko beam with enhanced stress recovery and constitutive relations. *Composite Structures 229*, 111265.

[13] Balkaya, C. (2001). Behavior and modeling of nonprismatic members having T-sections. *Journal of Structural Engineering 127*, 940–946.

[14] Balkaya, C., E. Citipitioglu, A. Tena-Colunga, and A. Tena-Colunga (1996). Stiffness formulation for nonprismatic beam elements. *Journal of Structural Engineering 122*(12), 1484–1489.

[15] Beltempo, A., G. Balduzzi, G. Alfano, and F. Auricchio (2015). Analytical derivation of a general 2d non-prismatic beam model based on the Hellinger–Reissner principle. *Engineering Structures 101*, 88–98.

[16] Beltempo, A., C. Cappello, D. Zonta, A. Bonelli, O. Bursi, C. Costa, and W. Pardatscher (2015). Structural health monitoring of the Colle Isarco viaduct. In *Environmental and Energy and Structural Monitoring Systems (EESMS) and 2015 IEEE Workshop on*, pp. 7–11. IEEE.

[17] Bennati, S., P. Bertolini, L. Taglialegne, and P. S. Valvo (2016). On shear stresses in tapered beams. In *GIMC-GMA 2016-XXI Convegno Nazionale di Meccanica Computazionale e VIII Riunione Gruppo Materiali AIMETA*, pp. 83–84. Tipolitografia Contini.

[18] Bertolini, P., M. Eder, L. Taglialegne, and P. Valvo (2019). Stresses in constant tapered beams with thin-walled rectangular and circular cross sections. *Thin walled structures 137*, 527–540.

[19] Bleich, F. (1932). *Stahlhochbauten*, Chapter 16, pp. 80–85. Verlag von Julius Springer.

[20] Blodgett, O. (1966). *Design of welded structures*, Chapter 4.4, pp. 1–8. the James F. Lincon arc welding foundation.

[21] Boley, B. (1963). On the accuracy of the Bernoulli-Euler theory for beams of variable section. *Journal of applied mechanics 30*(3), 373–378.

[22] Bournas, D. A., P. Negro, and F. F. Taucer (2014). Performance of industrial buildings during the emilia earthquakes in northern italy and recommendations for their strengthening. *Bulletin of Earthquake Engineering 12*(5), 2383–2404.

[23] Browns, C. (1984). Approximate stiffness matrix for tapered beams. *Journal of Structural Engineering 110*, 3050–3055.

[24] Bruhns, O. (2003). *Advanced Mechanics of Solids*. Springer.

[25] Computer & Structures Inc. (2011). *SAP2000 Version 21.0.2 - CSI Analysis Reference Manual*. Computer & Structures Inc.

[26] Dufour, J.-E., P. Antolin, G. Sangalli, F. Auricchio, and A. Reali (2018). A cost-effective isogeometric approach for composite plates based on a stress recovery procedure. *Composites Part B: Engineering 138*, 12–18.

[27] Eisenberger, M. (1985). Explicit stiffness matrix for nonprismatic members. *Computer & Structures 20*, 715–720.
[28] El-Mezaini, N., C. Balkaya, and E. Citipitioglu (1991). Analysis of frames with nonprismatic members. *Journal of Structural Engineering 117*, 1573–1592.
[29] Failla, G. and N. Impollonia (2012). General finite element description for non-uniform and discontinuos beam element. *Archive of Applied Mechanics 82*, 43–67.
[30] Felippa, C. A. (2001). A historical outline of matrix structural analysis: a play in three acts. *Computers & Structures 79*(14), 1313–1324.
[31] Gimena, F., P. Gonzaga, and L. Gimena (2008a). 3d-curved beam element with varying cross-sectional area under generalized loads. *Engineering structures 30*(2), 404–411.
[32] Gimena, F., P. Gonzaga, and L. Gimena (2008b). Structural analysis of a curved beam element defined in global coordinates. *Engineering Structures 30*(11), 3355–3364.
[33] Gimena, L., F. Gimena, and P. Gonzaga (2008). Structural analysis of a curved beam element defined in global coordinates. *Engineering Structures 30*, 3355–3364.
[34] Hodges, D., C. Jimmy, W. Yu, D. Hodges, J. Ho, and W. Yu (2008). The effect of taper on section constants for in-plane deformation of an isotropic strip. *Journal of Mechanics of Materials and Structures 3*(3), 425–440.
[35] Hodges, D., A. Rajagopal, J. Ho, and W. Yu (2011). Stress and strain recovery for the in-plane deformation of an isotropic tapered strip-beam. *Journal of Mechanics of Materials and Structures 5*(6), 963–975.
[36] Jourawski, D. (1856). Sur le résistance d'un corps prismatique et d'une piece composée en bois ou on tôle de fer à une force perpendiculaire à leur longeur. In *Annales des Ponts et Chaussées*, Volume 12, pp. 328–351.
[37] Just, D. (1977). Plane frameworks of tapering box and I-section. *Journal of the Structural Division 103*(1), 71–86.
[38] Kosko, E. (1982). Uniform element modeling of tapered frame members. *Journal of the Structural Division 108*(1), 245–264.
[39] Kutiš, V., J. Murin, R. Belak, and J. Paulech (2011). Beam element with spatial variation of material properties for multiphysics analysis of functionally graded materials. *Computers & Structures 89*(11-12), 1192–1205.
[40] Maplesoft (2019). *MAPLE 2018.1 - Maple User Manual*. Maplesoft.
[41] Mercuri, V. (2018, 03). *Form and structural optimization: from beam modeling to 3D printing of reinforced concrete members*. Ph. D. thesis, University of Pavia.
[42] Mercuri, V., G. Balduzzi, D. Asprone, and F. Auricchio (2016). 2D non-prismatic beam model for stiffness matrix evaluation. In *Proceedings of the Word Conference on Timber Engineering*.
[43] Murin, J., M. Aminbaghai, J. Hrabovskỳ, V. Kutiš, and S. Kugler (2013). Modal analysis of the fgm beams with effect of the shear correction function. *Composites Part B: Engineering 45*(1), 1575–1582.
[44] Murin, J., J. Hrabovsky, M. Aminbaghai, R. Gogola, V. Goga, F. Janíček, and S. Kugler (2018). Modelling and simulation of power lines made of composite structures. *Composite Structures 183*, 286–298.
[45] Murin, J. and V. Kutiš (2002). 3d-beam element with continuous variation of the cross-sectional area. *Computers & structures 80*(3-4), 329–338.
[46] Orr, J. J., T. J. Ibell, A. P. Darby, and M. Evernden (2014). Shear behaviour of non-prismatic steel reinforced concrete beams. *Engineering Structures 71*, 48–59.
[47] Paglietti, A. and G. Carta (2007). La favola del taglio efficace nella teoria delle travi di altezza variabile. In *AIMETA*.
[48] Paglietti, A. and G. Carta (2009). Remarks on the current theory of shear strength of variable depth beams. *The Open Civil Engineering Journal 3*, 28–33.
[49] Patel, C. and G. Acharya (2016). Analytical determination of deflection of stepped cantilever rectangular beam under uniform load.
[50] Patton, A., J.-E. Dufour, P. Antolin, and A. Reali (2019). Fast and accurate elastic analysis of laminated composite plates via isogeometric collocation and an equilibrium-based stress recovery approach. *Composite Structures 225*, 111026.
[51] Piazza, M., R. Tomasi, and R. Modena (2005). *Strutture in legno – materiale, calcolo e progetto secondo le nuove normative europee*. Hoepli.
[52] Portland and Cement Association (1958). *Handbook of frame constants. Beam factor and moment coefficient for members of variable section*. Portland and Cement Associations.
[53] Rajagopal, A. (2014). *Advancements in rotor blade cross-sectional analysis using the variational-asymptotic method*. Ph. D. thesis, Georgia Institute of Technology.
[54] Rajagopal, A. and D. H. Hodges (2014). Asymptotic approach to oblique cross-sectional analysis of beams. *Journal of Applied Mechanics 81*(031015), 1–15.
[55] Raymond, R. and F. Wang (1988). Stiffnesses of nonprismatic member. *Journal of Structural Engineering 114*(2), 489–494.
[56] Romano, F. (1996). Deflections of Timoshenko beam with varying cross-section. *International journal of mechanical sciences 38*(8), 1017–1035.
[57] Romano, F. and G. Zingone (1992). Deflections of beams with varying rectangular cross section. *Journal of engineering mechanics 118*(10), 2128–2134.
[58] Rubin, H. (1999). Analytische Berechnung von Stäben mit linear veränderlicher Höhe unter Berücksichtigung von M- and Q- und N- Verformungen. *Stahlbau 68*, 112–119.
[59] Schneider, K.J., Albert, and A. (2014). *Bautabellen für Ingenieure: mit Berechnungshinweisen und Beispielen*. Bundesanzeiger Verlag GmbH.
[60] Shooshtari, A. and R. Khajavi (2010). An efficient procedure to find shape functions and stiffness matrices of nonprismatic Euler-Bernoulli and Timoshenko beam elements. *European Journal of Mechanics A/Solids 29*, 826–836.
[61] SIMULIA Dassault Sistemes (2012). *Abaqus/CAE 2016 - Analysis User's Manual*. SIMULIA Dassault Sistemes.

[62] Tena-Colunga, A. (1996). Stiffness formulation for nonprismatic beam elements. *Journal of Structural Engineering 122*, 1484–1489.
[63] Tena-Colunga, A. and L. Becerril (2012). Lateral stiffness of reinforced concrete moment frames with haunched beams. In *15TH WORLD CONFERENCE ON EARTHQUAKE ENGINEERING*.
[64] Timoshenko, S. and J. N. Goodier (1951). *Theory of Elasticity* (Second ed.). McGraw-Hill.
[65] Timoshenko, S. P. and D. H. Young (1965). *Theory of Structures*. McGraw-Hill.
[66] Trahair, N. and P. Ansourian (2016). In-plane behaviour of web-tapered beams. *Engineering Structures 108*, 47–52.
[67] Trinh, T. and B. Gan (2015). Development of consistent shape functions for linearly solid tapered Timoshenko beam. *Journal of Structural and Construction Engineering 80*, 1103–1111.
[68] Tudjono, S., A. Han, N. Dinh-Kien, K. Shota, and G. S. Buntara (2017). Exact shape functions for Timoshenko beam element. *Journal of Computer Engineering 19*(3), 12–20.
[69] Velázquez Santillán, F., A. Luévanos Rojas, S. López Chavarría, and M. Medina Elizondo (2019). Modeling for beams of rectangular cross section with parabolic haunches: Part 1. *Computación y Sistemas 23*(2), 547–556.
[70] Vu-Quoc, L. and P. Léger (1992). Efficient evaluation of the flexibility of tapered I-beams accounting for shear deformations. *International journal for numerical methods in engineering 33*(3), 553–566.
[71] Weeger, O., S.-K. Yeung, and M. L. Dunn (2018). Fully isogeometric modeling and analysis of nonlinear 3d beams with spatially varying geometric and material parameters. *Computer Methods in Applied Mechanics and Engineering 342*, 95–115.
[72] Wong, F. T., J. Gunawan, K. Agusta, H. Herryanto, and L. S. Tanaya (2019). On the derivation of exact solutions of a tapered cantilever timoshenko beam. *Civil Engineering Dimension 21*(2), 89–96.
[73] Yang, Y., J. Orr, T. Ibell, and A. Darby (2015). Shear strength theories for beams of variable depth. In *Proceedings of IASS Annual Symposia*, Volume 2015, pp. 1–11. International Association for Shell and Spatial Structures (IASS).
[74] Yang, Y., J. Orr, and S. Spadea (2018). Shear behavior of variable-depth concrete beams with wound fiber-reinforced polymer shear reinforcement. *J. Compos. Constr 22*(6), 04018058.
[75] Zeinali, Y., S. Jamali, and S. Musician (2013). General form of the stiffness matrix of a tapered-beam column. *International Journal of Mining and Metallurgy & Mechanical Engineering 1*, 2320–4060.
[76] Zhi-Luo, Y., X. Xu, and F. Wu (2007). Accurate stiffness matrix for nonprismatic members. *Journal of Structural Engineering 133*, 1168–1175.
[77] Zhou, M., J. Zhang, J. Zhong, and Y. Zhao (2016). Shear stress calculation and distribution in variable cross sections of box girders with corrugated steel webs. *Journal of Structural Engineering 142*(6), 04016022.
[78] Zienkiewicz, O. and R. Taylor (2005). The finite element method. In *For solid and structural mechanics*. Elsevier.
[79] Zienkiewicz, O., R. Taylor, and J. Zhu (2005). The finite element method. In *Its basis and fundamentals* (V ed.). Elsevier.